MONITORING DEFORMATION OF SHRINKABLE MATERIALS DURING DRYING USING IMAGE ANALYSIS

A THESIS SUBMITTED IN FULFILLMENT
OF THE REQUIREMENTS FOR THE DEGREE OF
MASTER OF ENGINEERING IN FOOD ENGINEERING
FACULTY OF ENGINEERING
KING MONGKUT'S INSTITUTE OF TECHNOLOGY LADKRABANG
2018

KMITL-2018-EN-M-270-028

MONITORING DEFORMATION OF SHRINKABLE MATERIALS DURING DRYING USING IMAGE ANALYSIS

ANYANUN STIENKIJUMPAI

A THESIS SUBMITTED IN FULFILLMENT
OF THE REQUIREMENTS FOR THE DEGREE OF
MASTER OF ENGINEERING IN FOOD ENGINEERING
FACULTY OF ENGINEERING
KING MONGKUT'S INSTITUTE OF TECHNOLOGY LADKRABANG
2018

KMITL-2018-EN-M-270-028

การเฝ้าสังเกตการเปลี่ยนรูปของวัสดุหดตัวได้ขณะอบแห้ง โดยใช้การวิเคราะห์ภาพ

MONITORING DEFORMATION OF SHRINKABLE MATERIALS DURING DRYING USING IMAGE ANALYSIS

อัญญนันท์ เสถียรกิจอำไพ
ANYANUN STIENKIJUMPAI

วิทยานิพนธ์นี้สำหรับการศึกษาตามหลักสูตรปริญญาวิศวกรรมศาสตรมหาบัณฑิต
สาขาวิชาวิศวกรรมอาหาร
คณะวิศวกรรมศาสตร์
สถาบันเทคโนโลยีพระจอมเกล้าเจ้าคุณทหารลาดกระบัง
พ.ศ. 2561

KMITL-2018-EN-M-270-028

THESIS CERTIFICATION

FACULTY OF ENGINEERING

KING MONGKUT'S INSTITUTE OF TECHNOLOGY LADKRABANG

Thesis Title Monitoring Deformation of Shrinkable Materials during Drying using Image Analysis

Student Miss Anyanun Stienkijumpai

Student Id. 57601284

Degree Master of Engineering

Program Food Engineering

Thesis Advisor Dr Maturada Jinorose

Thesis Reference Number KMITL-2018-EN-M-270-028

EXAMINERS		SIGNATURES
Prof Dr Sakamon	Devahastin	
Asst. Prof Dr Maradee	Phongpipatpong	
Asst. Prof Dr Teerin	Chysirichote	
Dr Varesa	Chuwattanakul	
Dr Maturada	Jinorose	

Date 15th June 2018 **Time** 01:00 – 03:00 PM

Place Building A , 5th Floor Conference room no.3

(Assoc. Prof Dr. Komsan Maleesee)

Dean, Faculty of Engineering

15th June 2018

หัวข้อวิทยานิพนธ์	การเฝ้าสังเกตการเปลี่ยนรูปของวัสดุหดตัวได้ขณะอบแห้งโดยใช้การวิเคราะห์ภาพ
นักศึกษา	นางสาวอัญญนันท์ เสถียรกิจอำไพ
รหัสประจำตัว	57601284
ปริญญา	วิศวกรรมศาสตรมหาบัณฑิต
สาขาวิชา	วิศวกรรมอาหาร
พ.ศ.	2561
อาจารย์ที่ปรึกษาวิทยานิพนธ์	ดร.มธุรดา จิโนรส

บทคัดย่อ

การเปลี่ยนรูปของวัสดุเป็นปรากฏการณ์หนึ่งที่มักเกิดขึ้นในระหว่างการอบแห้ง โดยทั่วไป มักประเมินการเปลี่ยนรูปและรายงานผลในรูปของการหดตัวเชิงปริมาตร อย่างไรก็ตาม การหดตัวเชิงปริมาตรไม่สามารถใช้บอกการเปลี่ยนรูปแบบไม่เป็นเอกรูป ซึ่งมักเกิดขึ้นในระหว่างการอบแห้งวัสดุที่หดตัวได้ เช่น พอลิเมอร์ชีวภาพ ผักและผลไม้ งานวิจัยนี้จึงได้พัฒนาขั้นตอนวิธีและซอฟต์แวร์เพื่อสร้างภาพสามมิติโดยการประกอบภาพสองมิติที่ถ่ายจากหลาย ๆ มุม และเฝ้าสังเกตการเปลี่ยนแปลงแบบไม่เป็นเอกรูปจากภาพที่สร้างขึ้น วัสดุที่ใช้ในการทดสอบ คือ วุ้นซึ่งมีปริมาณน้ำตาลแตกต่างกันและอบแห้งด้วยอัตราที่แตกต่างกัน ทั้งนี้ ตรวจสอบความสมเหตุสมผลของขั้นตอนวิธีการสร้างภาพที่พัฒนาขึ้นด้วยรูปทรงเรขาคณิตพื้นฐาน จากนั้นคำนวณพารามิเตอร์เชิงภาพต่าง ๆ ทั้งในสองมิติ ได้แก่ พื้นที่แบบฉายต่าง ๆ เส้นรอบรูปต่าง ๆ ความยาวในหลากหลายแกน เส้นผ่านศูนย์กลางสมมูล เส้นผ่านศูนย์กลางทางสถิติของ Feret ตัวประกอบรูปทรง ความกลม ขอบเขต ความเป็นทรงกลม ความตันของภาพ ความคอนเวกซ์ ความเยื้องศูนย์กลาง อัตราส่วน ความเรียบ ความยืด ความเป็นสี่เหลี่ยม และมิติสาทิสรูป (Fractal dimension) และในสามมิติ ได้แก่ ปริมาตร พื้นที่ผิว ภาวะทรงกลม ภาวะทรงกลมของ Wadell ความกลมของ Wadell อัตราส่วนรัศมี และเอนโทรปีรูปร่างของ Hoffmann และทดสอบความเหมาะสมในการใช้พารามิเตอร์ต่าง ๆ เหล่านี้โดยการเฝ้าสังเกตการเปลี่ยนรูปทรงวัสดุระหว่างการอบแห้ง จากผลการทดลองพบว่าสามารถใช้ค่าขอบเขตในการระบุจุดเริ่มต้นของการเปลี่ยนแปลงรูปแบบไม่เป็นเอกรูปตลอดจนใช้เฝ้าสังเกตการเปลี่ยนรูปในสองมิติได้ดี ในกรณีการใช้งานในสามมิติ ค่าภาวะทรงกลมเป็นพารามิเตอร์ที่ใช้งานได้ดี

คำสำคัญ : วัสดุชีวภาพ, ค่าขอบเขต, ตัวประกอบบ่งรูปร่าง, น้ำตาล, การหดตัว

Thesis	Monitoring Deformation of Shrinkable Materials during Drying using Image Analysis
Student	Miss Anyanun Stienkijumpai
Student ID.	57601284
Degree	Master of Engineering
Program	Food Engineering
Year	2018
Thesis Advisor	Dr. Maturada Jinorose

ABSTRACT

Deformation is a phenomenon that is common during drying. Generally, deformation is evaluated and reported in terms of volumetric shrinkage. However, volumetric shrinkage cannot be used to describe non-uniform deformation, which commonly takes place during drying of shrinkable materials such as biopolymers, fruits and vegetables. In this study, algorithms and software were developed to first reconstruct 3D images from 2D images and then to monitor non-uniform deformation of such images. Agar gel with different sugar contents were used as the test materials and allowed to undergo drying at different rates. The developed image reconstruction algorithms were first validated with standard geometrical shapes. Various image-based parameters, both in two dimensions, i.e., projected area, perimeter, length in many axes, equivalent diameter, Feret's statistical diameter, form factor, roundness, extent, circularity, solidity, convexity, eccentricity, ratio, entirety, elongation, rectangularity and fractal dimension (using box counting method); and in three dimensions, i.e., volume, surface area, sphericity, Wadell's roundness, radius ratio and Hoffmann shape entropy, were then calculated and assessed for their suitability to monitor non-uniform shrinkage of the materials undergoing drying. Result showed that extent could be used to identify the onset and to monitor non-uniform deformation in two dimensions, while sphericity could be used for such tasks in three dimensions

Keywords: Biomaterial, Extent, Shape Factor, Sugar, Shrinkage

ACKNOWLEDGEMENTS

I would like to express my sincerely appreciation to my academic advisor, Dr. Maturada Jinorose for her valuable and constructive suggestions during the planning, development and conduct of this thesis. Her willingness to devote her time so generously is indeed very much appreciated.

I would also like to offer my gratitude to Prof. Dr. Sakamon Devahastin. Advices given by him are of a great help in the planning and analysis of the results.

My special thanks are extended to the staff of the Department of Food Engineering, KMITL for providing information and to NECTEC Pilot Plant for supporting the use of the 3D light scattering scanner. My appreciation also goes to the Thailand Research Fund (TRF) for supporting the study financially through the new Research Grant (Grant no. TRG5880109)

Last, but certainly far from the least, I am grateful to my family and friends for their unfailing support and continuous encouragement throughout the many years of my study and through the process of researching and writing this thesis. My accomplishment would not have been possible without their support.

TABLE OF CONTENTS

TABLE OF CONTENTS (CONT'D)

LIST OF TABLES

LIST OF FIGURES

LIST OF FIGURES (CONT'D)

LIST OF FIGURES (CONT'D)

NOMENCLATURE

Symbol

A	Projected area of 2D image	Pixel
B	Blue value in RGB color space	
D	Average diameter of sample	mm
D_f	Feret's statistical diameter (Feret diameter) of 2D image	Pixel
D_1	Longest length between two surface area points	mm
D_2	Longest length between two surface area points that is perpendicular to D_1	mm
D_3	Longest length between two surface area points that is perpendicular to D_1 and D_2	mm
D_{eqv}	Equivalent diameter	
Diff	Difference of parameter between two methods	
G	Green value in RGB color space	
h	Average height of sample	mm
L	Bounding box length of 2D image	Pixel
m	Mass of sample	g
Major	Major axis length of 2D image	Pixel
MR	Moisture ratio	
Minor	Minor axis length of 2D image	Pixel
n	Number of all data	
P	Interested parameters	
Perim	Perimeter of 2D image	Pixel
R	Red value in RGB color space	
r	Radius between edge and center of sample	Pixel
SA	Surface area of sample	Mesh, mm^2
SA_{sphere}	Surface area of sphere with same image-based volume of sample	Mesh
V	Volume of sample	Voxel, mm^3
W	Bounding box width of 2D image	Pixel
x	Data	
$\overline{x}$	Average data	

NOMENCLATURE (CONT'D)

Greek letter

ρ	Density of solvent	g/mm^3

Subscript

0	Value from initial point
2D	From 2D image analysis method
3D	From 3D image analysis method
bd	Bone dry
box	Parameter from bounding box of sample
C	From calculation method
cvx	Parameter from convex area
eq	Equilibrium
ef	Parameter from ellipse that has same major and minor axis lengths with sample
i	Number of data
l	From liquid displacement method
max	Maximum value
mean	Average value
min	Minimum value
s	Solvent

CHAPTER 1
INTRODUCTION

1.1 Statement and Significance of the Problem

Drying is a process that removes a solvent (mostly water) from a material and turns it into a solid product [1]. Many changes occur during drying, i.e., physical, chemical and microstructural changes. Deformation (i.e., change of shape and/or size), is one of the changes that commonly occurs [2]. Generally, deformation is quantified by direct measurement using such instruments as Vernier caliper [3] or evaluated and reported in terms of the volumetric shrinkage, which can be calculated from the ratio of the material volume at any instant to the initial volume; such simple methods as solid or liquid displacement method can be employed to determine the volumetric shrinkage [4].

However, volumetric shrinkage, which is popularly used because of its simplicity, cannot be used to describe non-uniform deformation, which commonly takes place during drying of highly shrinkable materials such as biopolymers and even fruits and vegetables [5]. It has indeed been reported that different drying methods can cause different patterns of deformation even when applied to the same material. In such a case, the volumetric shrinkage of the two samples may be similar, but their shapes may be much different [6, 7]. Since shape of a material can affect the heat and mass transfer, which in turn affects the physical, physicochemical, microstructural and nutritional properties of a dried product, it is important to be able to measure how shape (and not only size or volume) of a material changes during drying.

Although image analysis has long been applied to describe deformation and various shape factors have been proposed for such a purpose, most of the reported works were performed using shape factors that describe deformation in only one or two dimensions. This has been done despite the well known fact that deformation usually occurs in all three directions. This is because 2D image acquisition and analysis is much easier than that of 3D images [8]. Recently, however, limited attempts have been made to describe shape using indicators derived from 3D image-based information. For example, Bullard and Garboczi [9] reported that any properties, including volume, dimension and sphericity of 3D-shaped particles (star-shape) could be calculated from a mathematical model developed from macroscopic parameters and surface integrals. Various sphericity-based shape factors, i.e., true roundness, sphericity, radius ratio of bounding sphere, Hofmann shape entropy, Wadell's roundness and Wadell's sphericity, were indeed calculated from the particle surface integrals. It was found that the roundness could capture the particle shape better

than the other tested shape factors. Radivillaite et al. [10] who attempted to characterize various grain shapes, i.e., chickpea, maize and bean, also found that a mathematical model developed from spherical harmonics could be used to classify the shape rather well. It must be noted nevertheless that the shape identification or characterization has usually been done only on standard or drawn-shapes; real materials with complex shapes have not been tested due to the limitation of image acquisition algorithms.

Although there currently exists several software such as Autodesk Recap 360 (Autodesk Inc., San Rafael, CA), Agisoft Photoscan (Agisoft, LLC, St. Petersburg, Russia) or Visual SFM (http://ccwu.me/vsfm/) that can be used to construct 3D images from 2D images, ready-made reconstructed 3D images are in most cases incomplete and must be further adjusted and calibrated if accurate information including shape, volume and surface are to be obtained and, in particular, quantified. Since deformation occurs in all dimensions, 3D image-based analysis should more accurately represent non-uniform deformation than a simpler 2D image-based method.

In this study, algorithms and software were developed to first reconstruct 3D images from 2D images; standard geometrical shapes were used for the validation and calibration purposes. Various parameters, both in two dimensions, i.e., projected area, perimeter, length in many axes, equivalent diameter, Feret's statistical diameter, form factor, roundness, extent, circularity, solidity, convexity, eccentricity, ratio, entirety, elongation, rectangularity and fractal dimension (using box counting method); and in three dimensions, i.e., volume, surface area, sphericity, Wadell's roundness, radius ratio and Hoffmann shape entropy, were then calculated and compared to determine if they have the capability of monitoring non-uniform deformation. Agar gel with different sugar contents were used as the test materials and allowed to undergo drying at different rates.

1.2 Objectives

1 To investigate if image analysis can be used as a tool to monitor non-uniform deformation.

2 To propose suitable parameters that can be used to evaluate deformation characteristics of a model food material.

3 To test and compare the results obtained through the use of the proposed parameters and those obtained via the traditional evaluation methods.

4 To establish relationships between the drying condition as well as food composition and non-uniform deformation of the test material during drying.

1.3 Scope of the Study

1 Investigating if image analysis can be used as a tool to monitor non-uniform deformation. This involved the following steps of the study:
   - Setting up an image analysis system and developing algorithms to evaluate the various kinds of dimensions (i.e., projected area, perimeter, image-based volume and surface area) and shape (i.e., deformation) changes during drying.
   - Agar gel (with different sugar content: 0%, 10% and 20%) was used as test material.
   - Using drying temperature of 60 °C and 80 °C.

2 Proposing suitable parameters that can represent non-uniform deformation characteristics of the test materials and also represent degree of volumetric shrinkage and capture both dimension and shape changes in three dimensions.

3 Testing and comparing the results obtained through the use of the proposed parameters and via the use of the traditional evaluation methods, i.e., volumetric shrinkage, fractal dimension and other conventional shape factors.

4 Establishing the relationships between the drying temperature as well as food composition and non-uniform deformation of the test material during drying.

1.4. Expected Benefits

The obtained information should be useful for future development of a real-time and/or in situ monitoring and control system of a drying process for high-value foods and soft biomaterials via the use of a computer vision system.

CHAPTER 2
BACKGROUND

2.1 Property Changes during Drying

Most changes food experiences during drying occur due to moisture loss [1, 11]. Such changes could be classified into two groups, consisting of physical and chemical property changes. Physical properties (especially size, shape and even color) are of primary importance because they directly affect the decision of consumers regarding the quality of a product. In the case of chemical properties, even if some of them cannot be observed by eyes, these properties are important as they indicate how long a product can be stored without spoilage or expiration; these properties are also in most cases directly related to other important properties (including in fact the physical properties) of a product as well. Chemical changes are nevertheless not of focus in this study.

2.1.1 Physical Property Changes

Physical changes directly affect the buying behavior of customers since these properties, including size, shape and color, can be visually observed. Understanding and monitoring of physical property are therefore of great importance and must be carefully performed. In this work, only the changes in size and shape will be focused, however.

Change of Size during Drying

There are two major types of changes in size, i.e., swelling and shrinkage. For example, upon baking, bread experiences swelling. Its size would become larger as a result of gas production by yeasts. Upon drying, however, most foods or biomaterials suffer shrinkage. Shrinkage occurs when a material experiences the moisture losses. Upon the losses of water, the remaining structure, which mainly consist of cell walls and cell membrane, would start to collapse, causing the material to shrink [11].

Normally, shrinkage is reported in terms of the ratio between the volume of a material at any instant to its initial volume, the so-called ‘volumetric shrinkage’. Volumetric shrinkage is generally measured using a liquid displacement method

Change of Shape during Drying

There are two types of shape changes (or deformation), including uniform deformation and non-uniform deformation. Uniform deformation is the phenomenon that takes place when the size of a material changes while the shape still remains the same. On the other hand, when the size as well as shape of a material change as shown in Figure 2.1, deformation is said to be non-uniform. This occurs as a result of

the moisture gradients within the microstructure. When moisture is being removed during drying, the rate of removal is not equal at every position. Such non-uniformity in moisture removal would naturally lead to non-uniformity in shrinkage as well [11].

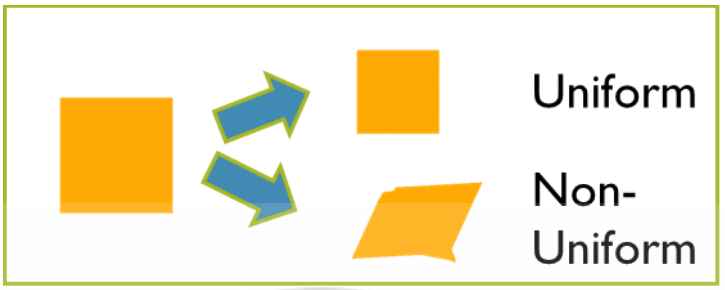

Figure 2.1 Difference between uniform and non-uniform deformation

Although volumetric shrinkage has extensively been used to quantify deformation, it is not appropriate when non-uniform deformation is involved. Devahastin et al. [6] and Devahastin and Niamnuy [7] indeed suggested that volumetric shrinkage might not provide accurate description of deformation if the volume does not change. There are in fact many other parameters that can better indicate the change of shape, including many shape factors that will later be discussed.

2.2 Image Analysis Techniques

From all 5 sensations, vision is the most believable comparing to scent, voice, taste and touch [12]. Visual information is, however, subjective as it depends on how individual brain interprets the data based on one's experience [13, 14]. Additionally, human can only see within the wavelength range of 400 and 700 nm [12]. A computer vision system (CVS) has therefore been developed to alleviate the aforementioned limitations of human eyes and brain. CVS employs a digital camera or other similar image acquisition tools to capture an image prior to analyzing via the use of computer (running with appropriate software or algorithms). CVS can therefore compare the objects without any bias or alteration. For this reason, a CVS can provide quantitative data instead of qualitative data, and it is more appropriate for objective measurement and evaluation.

2.2.1. 2D Image Acquisition

Both humans and CVS need 3 common components to observe something, which are light, object and receiving sensor as shown in Figure 2.2. Different types of lights are available based on the wavelength, which in turn affect the perceived color. In general, D_{65} is a standard lightsource of a CVS since it represents average light as

shown in Figure 2.3 [15]. Besides the type of the light, the angle between the light and an object is also importance. 45° is usually selected for image acquisition purpose [16]; see Figure 2.4. Moreover, when the light hits on an object, reflection or refraction would occur. However, how such a phenomenon would occur depends on the character of the surface of an object. If the surface is shiny or glossy, reflection would occur. Therefore, shiny and glossy objects are not suitable for CVS-based analysis; lightness would be a affected and the analyzed may be adversely affected. Lastly, reflection of light from an object must travel to a receiving sensor such as eyes or camera for the acquisition to really take place.

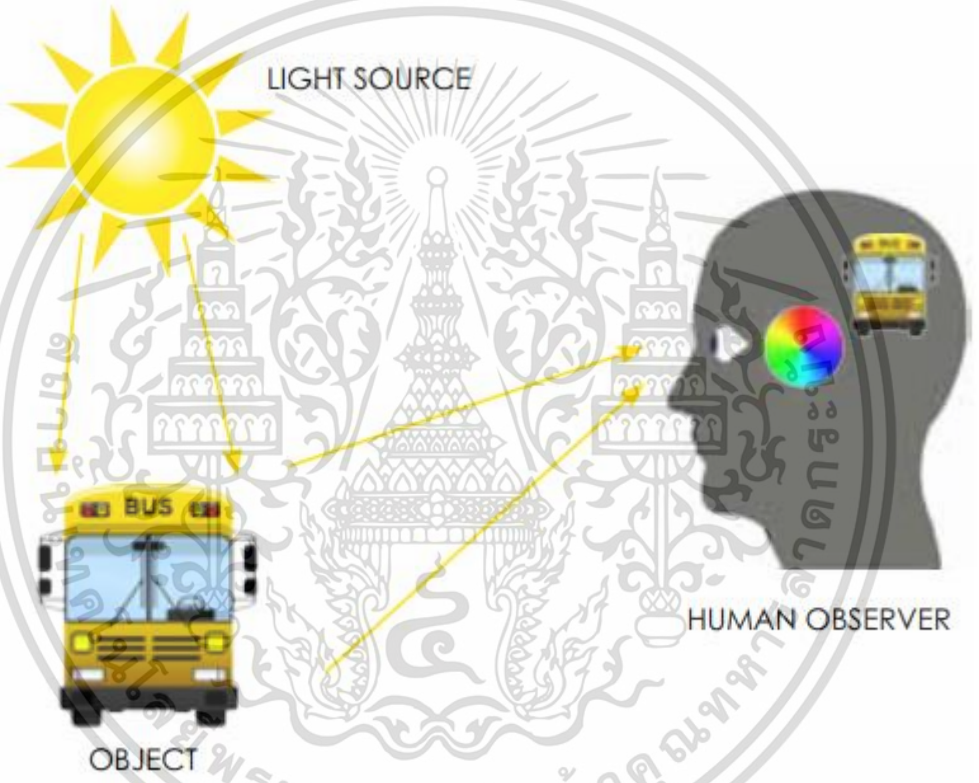

Figure 2.2 Relation between light source (the sun), object (a bus) and receiving sensor (eyes of human) [17]

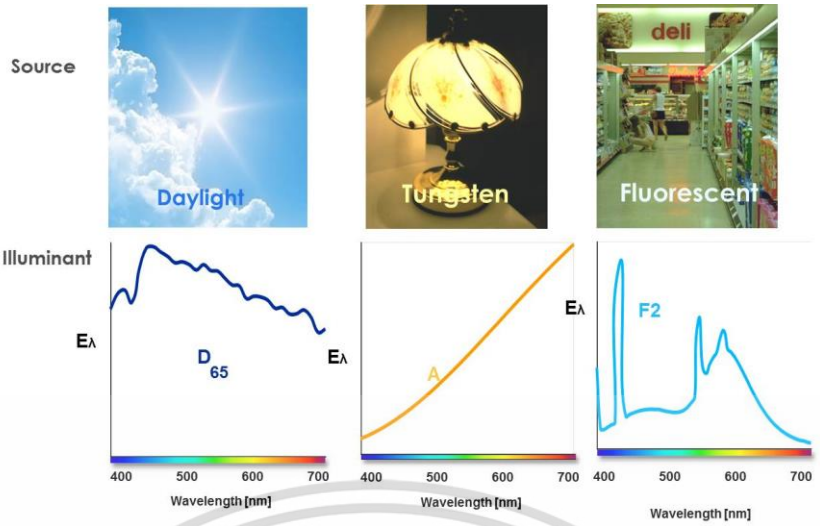

Figure 2.3 Types of light sources and their wavelengths [18]

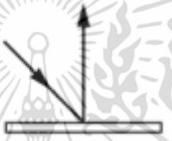

Figure 2.4 45° Angle between light source and object [16]

As mentioned earlier, an image capturing component with a CVS can be a digital camera, scanner, machine vision system or digital microscope based on the type of data to be acquired. Digital camera could be used for proper works such as analyzing apple during drying [19]. Scanner can be applied for a powdery product [20]. Machine vision could be used for capturing images during a continuous process, while digital microscope is applied for tiny objects. These devices could not nevertheless capture an image without a sensor. Many types of sensors are available, even for the same capturing system. For example, complementary metal-oxide semiconductor (CMOS) and charge couple device (CCD) for a digital camera and contact imaging sensor (CIS) and CCD for a scanner.

In the case of a digital camera, a CCD chip contains an array of diodes as shown in Figure 2.5. When a CCD sensor captures the light, the semiconductor raises electrons from the valence to conduction band. Light intensity is directly measured as the number of electrons (Figure 2.5 (a)). So, the advantage of this sensor is that no image distortion would occur; this type of sensor, however, requires more power. In contrast, as shown in the Figure 2.5 (b), a CMOS chip is organized as a computer memory chip. When diodes detect the light, electrons are read out and addressed as row and column. Thus, a CMOS can operate faster and consumes less power comparing with a CCD [12].

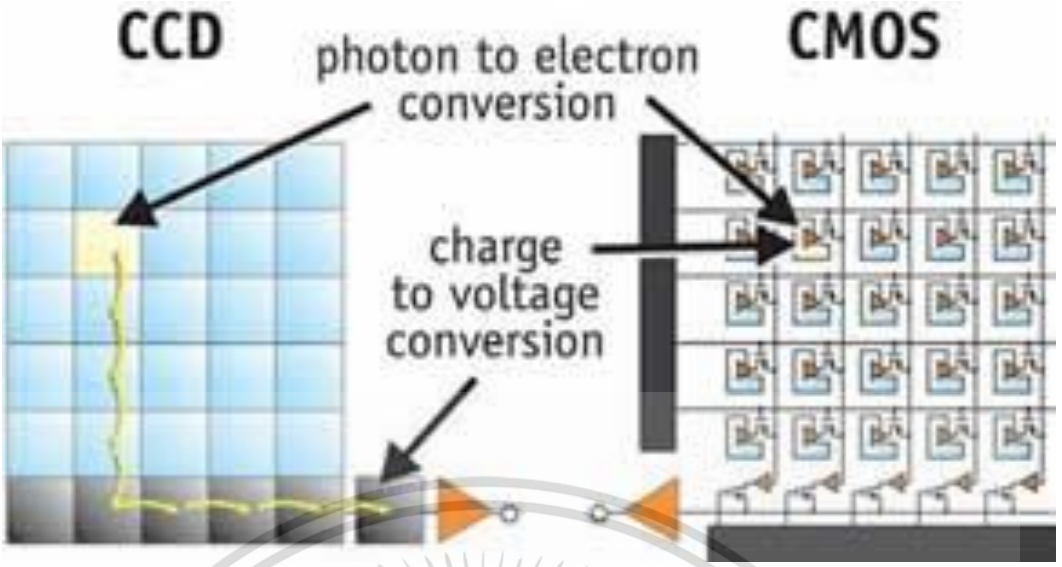

(a) (b)

Figure 2.5 Working principal of camera sensor. (a) CCD; (b) CMOS [21]

Camera functions are another important aspects that need careful attention. These functions consists of ISO, aperture and shutter speed. Figure 2.6 shows the effects on changing these functions in order to take a photo. Aperture is a hole of lens which controls the light and the depth of field [22]. Small aperture or less depth of field would provide sharp foreground and background. Large aperture or greater depth of field, however, would illustrate sharp foreground but blur background. Shutter speed or exposure time is the speed in capturing the light within the specified time [23]. To capture a fast moving object, fast shutter speed is needed to obtain a sharp image and slow shutter speed to obtain a blur picture. Lastly, ISO is the light sensitivity level [24].

Using a suitable sensor and photo setting would provide an image of good quality. However, there can still be some uncontrollable defects such as noise and blurred spots appearing on an acquired image. These defects must be corrected or pre-processed prior to image analysis.

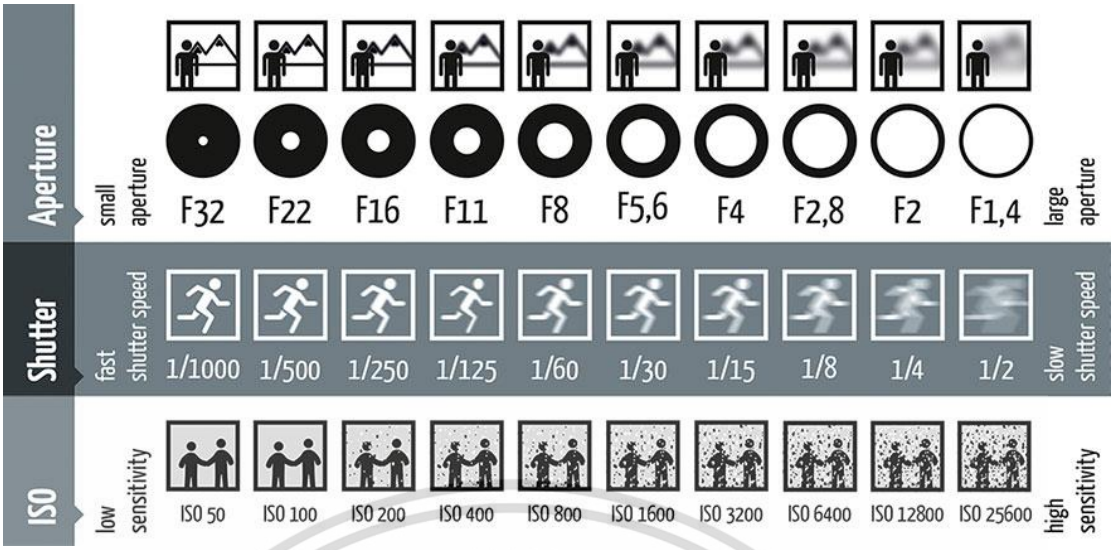

Figure 2.6 Images acquired at different values of ISO, aperture and shutter speed [25]

2.2.2 2D Image Pre-Processing

There are five characters of defects that can typically observed in an image. The first defect is noise, which can be further divided into two groups, consisting of speckle noise and periodic noise. Speckle noise or pixel point occurs where there is irregular light, and it can be handled by a median filter. Periodic noise, which is an irregularity from the acquiring process, can be managed by many methods such as Gaussian blur, median filter or top-hat filter. Secondly, abnormal distribution of light from the source of light can be fixed by taking only a background image, then applying it to eliminate a picture of foreground and background. The third defect is image distortion, which affects the size and shape of an image. This type of defect can be handled by taking an image with a regular grid. However, most cameras have an automatic calibration to take care of this defect. Fourthly, blur on an image can be fixed by Fourier transform. Lastly, unwanted objects on an image can be eliminated by selecting/cropping an area of interest. This also leads to a smaller picture, which can help save the time of process and storage space on a computer [14].

2.2.3 2D Image Segmentation

Image segmentation is the method to separate foreground from background. A segmented image is usually a binary image, with values of 1 and 0 set for foreground and for background, respectively. There are many methods for segmentation; the choice depends on the characteristics of an object. For example, watershed method might be appropriate for a large quantity of objects, so there is less background. Nevertheless, for Food engineering applications, the most suitable method is probably

the thresholding method, which separates foreground from background by an appropriate threshold value. There are two ways to determine a threshold value. The value can be determined based on the most appropriate value that can be used to separate foreground from background. Another method is based on calculation, using such method as the Otsu's method, which chooses a threshold value from the smallest value within class variance between foreground and background [26, 27]

2.2.4 2D Image Analysis

Image analysis is a process that extracts parameters from a selected image. 2D and 3D analyses are considerably different. 2D image analysis can extract both dimension parameters and data of color. The accuracy of the extracted dimension parameters relies on the process of segmentation, while the correctness of color data is based on the processes of acquiring an image as well as segmentation.

2.2.4.1 Dimension Parameters

These parameters indicate how large or how long a sample is; a ratio of these parameters could be used to measure shrinkage or swelling. For instance, Fernández et al. [19] showed that a decrease in the perimeter of apple slices in the period of dehydration could be connected to shrinkage.

Projected area Perimeter

There are two methods to determine both the projected area and perimeter of an object in a 2D image. The first method involves manual counting of pixel of an object to determine the projected area and of the edge to determine the perimeter. The second method involves the calculation of a pattern; this can be such methods as the 2-2 pixel neighbor method [28]. Figure 2.7 shows the projected area and perimeter calculated by both methods.

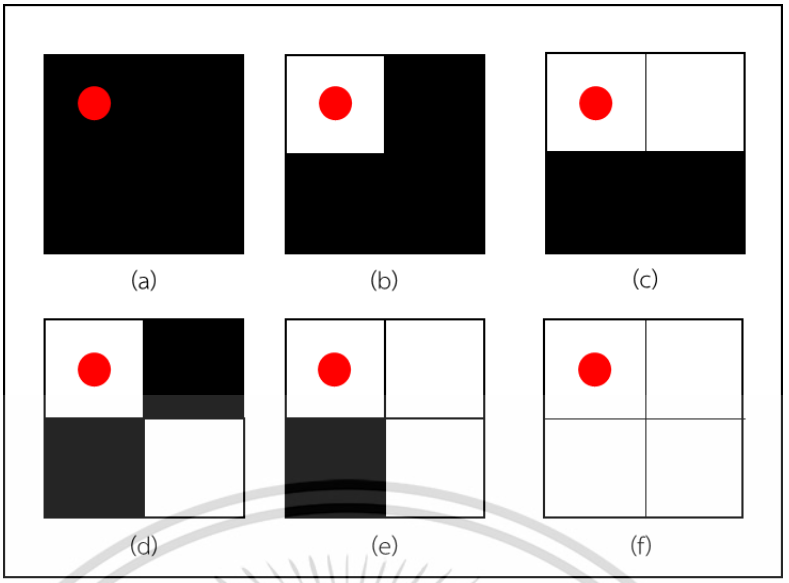

	Projected area		Perimeter	
	Self counting	2-2 Neighbor	Self counting	2-2 Neighbor
(a)	0	0	0	0
(b)	1	1/4	1	N/A
(c)	2	1/2	2	1
(d)	2	3/4	2	$\sqrt{2}$
(e)	3	7/8	3	2
(f)	4	1	N/A	N/A

Figure 2.7 Projected area and perimeter counts from different methods and positioning of white pixel where red dot is start pixel

Major Axis and Minor Axis Lengths

Major axis is the longest diameter of an ellipse that has the same normalized second central moment as the sample, while minor axis is the longest diameter that is perpendicular to the major axis [28]. Major and minor axes could be used to calculate the area of ellipse that has the same major and minor axis lengths by Equation 2.1 [29].

$$A_{\text{ef}} = \frac{\pi \cdot major \cdot minor}{4} \tag{2.1}$$

Feret's statistical Diameter and Equivalent Diameter

Feret's statistical diameter (Feret diameter) is the longest distance between any two points along a selected boundary; this is also known as a maximum caliper [30]. It could be used to measure the maximum diameter of an object. Equivalent diameter

is, on the other hand, the diameter of circle that has the same area as an object of interest. This can be calculated as per Equation 2.2 [27]

$$D_{\mathrm{eqv}} = \sqrt{\frac{4A}{\pi}} \tag{2.2}$$

Bounding Box and Convex Area

Bounding box is the smallest rectangle that an objected could fit in. In contrast, convex area is the area of the smallest enclose polygon that an object could fit in [28].

Radius, Circumscribed Radius and Inscribed Radius

Length between each pixel, which is on the edge of an object to the centroid of an object [27]. The longest radius can be considered as circumscribed radius, while the shortest radius can be considered as inscribed radius [14].

2.2.4.2 Shape Parameters

Since dimension parameters alone cannot be used to described shrinkage, various shape parameters have been developed to describe changes in shape of an object. Neal and Russ [14] categorize shape parameters into 4 types as follows.

Difference from Circle

A circle is used as a base shape because not only humans can easily imagine this simple shape, but in algorithms it is easy to assign to the calculation that all lengths from the center to each point on the edge are equal [14]. There are also many other parameters that are derived from this simple concept. The parameters that have been collected are listed below in Equations 2.3 to 2.13 [14, 28 ,29, 31].

$$\mathrm{Formfactor} = \frac{4\pi A}{Perim^2} \tag{2.3}$$

$$\mathrm{Roundness} = \frac{4A}{\pi {D_{\mathrm{f,max}}}^2} \tag{2.4}$$

$$\mathrm{Convexity}_{cvx} = \frac{Perim}{Perim_{\mathrm{cvx}}} \tag{2.5}$$

$$\mathrm{Eccentricity} = \frac{\sqrt{major^2 - minor^2}}{major} \tag{2.6}$$

$$\text{Circularity } = \frac{Perim}{2\sqrt{\pi A}} \tag{2.7}$$

$$\text{Convexity}_{\max} = \frac{\pi D_{\text{f,max}}}{Perim} \tag{2.8}$$

$$\text{Axial ratio} = \frac{Minor}{Major} \tag{2.9}$$

$$\text{Elongation} = \frac{{D_{\text{f,max}}}^2}{A} \tag{2.10}$$

$$\text{Feret major ratio} = \frac{D_{\text{f,min}}}{major} \tag{2.11}$$

$$\text{Square} - \text{circularity} = \frac{Perim^2}{A} \tag{2.12}$$

$$\text{Area per perimeter} = \frac{A}{Perim} \tag{2.13}$$

Stretching Out

In some cases, the different dimensions of an object may change disproportionally; for example, a circle may change into an ellipse. In such cases, using circle-based parameters may not be adequate as it would not be possible to tell how much length or width has indeed changed. So, stretching out parameters are created to alleviate the above-mentioned limitation. Equations 2.14 to 2.16 show how to calculate some stretching out parameters [14, 28 ,29, 31].

$$\text{Aspect ratio} = \frac{D_{\text{f,max}}}{D_{\text{f,min}}} \tag{2.14}$$

$$\text{Extent}_{\text{box}} = \frac{A}{LW} \tag{2.15}$$

$$\text{Major/perim} = \frac{major}{Perim} \tag{2.16}$$

Filled Out

If an object dose not stretch out but just experiences concave or convex at some points, filled out parameters can be used to indicate such changes [14]. For example, if an edge of a square is trimmed out, the square would still look like a square and does not stretch out. Equations 2.17 to 2.21 define selected filled out parameters [14, 28 ,29, 31].

$$\text{Extent}_{\max} = \frac{A}{\pi {r_{\max,2D}}^2} \tag{2.17}$$

$$\text{Solidity} = \frac{A}{A_{\text{cvx}}} \tag{2.18}$$

$$\text{Radius ratio} = \frac{r_{\min,2D}}{r_{\max,2D}} \tag{2.19}$$

$$\text{Entirety } = \frac{A_{\text{cvx}} - A}{A} \tag{2.20}$$

$$\text{Rectangularity}_{\text{ef}} = \frac{A_{\text{ef}}}{LW} \tag{2.21}$$

Roughness of Edge

If an edge of an object simply becomes rougher or smoother, roughness of edge might be a useful parameter. Roughness of edge parameters can be calculated as per Equations 2.22 to 2.28 [14, 28 ,29, 31].

$$\text{SD Radius} = \sqrt{\frac{\left(r_{\max,2D} - r_{\text{mean},2D}\right)^2 - \left(r_{\max,2D} - r_{\min,2D}\right)^2}{2}} \tag{2.22}$$

$$\text{Shape factor } = \frac{\text{SD Radius}}{r_{\text{mean},2D}} \tag{2.23}$$

$$\text{Perim/maxR } = \frac{Perim}{r_{\max}} \tag{2.24}$$

$$\text{Rectangularity}_{\text{box}} = \frac{Perim}{2L + 2W} \tag{2.25}$$

$$\text{Extent}_{\max,\min} = \frac{A}{D_{\text{f,max}} D_{\text{f,min}}} \tag{2.26}$$

$$\text{Paris factor} = 2\left(\frac{Perim - Perim_{\text{cvx}}}{Perim_{\text{cvx}}}\right) \tag{2.27}$$

$$\text{Concavity} = \sqrt{(1 - \text{solidity})^2 + \left(1 - \frac{1}{\text{Convexity}}\right)^2} \tag{2.28}$$

2.2.5 3D Image Processing and Acquisition

3D Image can show length, width and height of an object; this is different from 2D image that can show an image only in two dimensions. 3D image can be constructed by many such ways as via the use of a laser scanner, which is a popular method. Otherwise, 3D image can be reconstructed from 2D images taken at different positions and angles. Reconstruction a 3D image from multiple 2D images is clearly more convenient and cost effective as only a digital camera is mainly needed.

2.2.6 3D Image Analysis

3D image provides the data in the form of 'voxel' [12]; the data size is n x 3 where n is the number of voxel points and 3 represents the dimension that a point must be plotted. The data type is up to the type of an image. '.stl' file gives the point of mesh, while '.ply' gives the mesh itself.

2.2.6.1 Volume and Surface Area

Meshing is a key to calculate both the volume and surface area of a 3D image. Meshes give a 3D image a surface. Volume is then calculated by integrating the meshes, while surface area is calculated from the summary of the meshes. Comparing with results that can obtain via calculation using standard equations for volume and surface area, 3D image analysis provides more accurate volume and surface area data, especially in the case of an object with non-diagonal or convex shape. Note that calculation method is applicable only for standard geometric-shape objects. Although liquid displacement can provide adequate volume data of an object, the technique can never explain how a change in shape affects the volume of an object.

2.2.6.2 Shape Parameters

Both volume and surface area can be used to calculate a change in shape of an object. As in the case of a 2D image, shape of an object is usually compared with that of sphere. For example, sphericity, defined in Equation 2.29, which ranges from 0 to 1, indicates that an object is close to a sphere when the sphericity value is close to 1. Wadell's sphericity, defined in Equation 2.30, is the ratio of the surface area of an object to the surface area of an ellipse. Radius ratio$_{3D}$, Wadell's roundness and Hoffmann shape entropy, defined in Equations 2.31, 2.32 and 2.33, respectively, are based on the theory that a sphere has equally diameter. Scaling factor (Equation 2.34) is calculated the same way as sphericity [10, 14, 28].

$$\text{Sphericity} = \frac{(36\pi)^{\frac{1}{6}} V_{3D}^{\frac{1}{3}}}{SA_{3D}^{\frac{1}{2}}} \tag{2.29}$$

$$\text{Wadell's sphericity} = \frac{(4\pi)^{\frac{1}{3}}(3V_{3D})^{\frac{2}{3}}}{SA_{\text{sphere}}} \tag{2.30}$$

$$\text{Radius ratio}_{3\text{D}} = \frac{r_{\text{min,3D}}}{r_{\text{max,3D}}} \tag{2.31}$$

$$\text{Wadell's roundness} = \frac{\sum_{i=1}^{N}\left[\frac{r_{i,3\text{D}}}{r_{\text{max,3D}}}\right]}{N} \tag{2.32}$$

Hoffmann shape entropy

$$= \frac{1}{\ln\left(\frac{1}{3}\right)}\sum_{i=1}^{3}\left(\left(\frac{D_i}{D_1+D_2+D_3}\right)\ln\left(\frac{D_i}{D_1+D_2+D_3}\right)\right) \tag{2.33}$$

$$\text{Scaling factor} = \frac{{V_{3D}}^{\frac{1}{3}}}{{SA_{3\text{D}}}^{\frac{1}{2}}} \tag{2.34}$$

CHAPTER 3
RESEARCH METHODOLOGY

3.1 Materials Preparation

2% (w/w) granulated purified agar (Product no. 1016141000, Merck Millipore, Germany) was mixed with sugar (at mass ratio of 0%, 10% or 20%) and added to distilled water. The mixture was stirred at room temperature at 100 rpm for 1 h and then heated to 95 °C; stirring continued at 150 rpm for 10 min. The mixture was then allowed to cool for 10 min, after which it was poured into a silicone mold to form agar cubes with the dimensions of 1.9 cm x 1.9 cm x 1.9 cm. The cubes were taken out of the mold after 1 h setting at room temperature (25 °C ± 2 °C). The initial moisture content of agar gel with 0% sugar was 45.1% ± 0.5% (d.b.), while those of the gels with 10% and 20% sugar were 5.5% ± 0.2% (d.b.) and 2.7% ± 0.1% (d.b.) respectively.

3.2 Image Acquisition

Light box as shown in Figure 3.1 whose size was 40 cm x 40 cm x 40 cm with black matte paper inside was used. Four fluorescent lamps (FL8Wt5, 550 Flux, Daylight, 6500 K, Lamptan, Thailand) were placed on each side of the box. A compact camera (G16, Canon, Japan) was set at M-mode; aperture, shutter speed, ISO and image resolution were set at 8, 1/125 s, 200 and 1600 pixel x 1200 pixel, respectively. The camera was placed on the top at the centre of the corner of the box, with 45° / 0° according to ASTM E179 [16] standard. A sample was placed on a rotating platform (11 cm height), which was in turn placed on a static base (9 cm height). The sample was placed on a clear base on the top of the poles. Images were taken from 5 positions as shown in Figure 3.2; further explanation on image acquisition will be given in Section 4.1. Three-dimension image was reconstructed from the acquired 2D images using Autodesk Recap 360 software (Autodesk Inc., San Rafael, CA). MeshLab (Visual computing Lab. ISTI-CNR, http://www.meshlab.net) software was used to perform post-processing step for reducing unwanted objects.

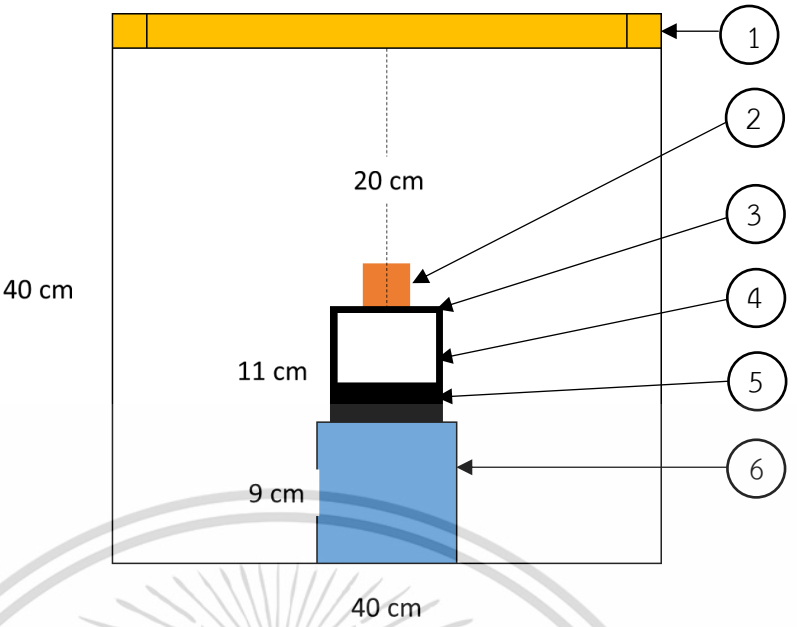

Figure 3.1 Light box with (1) Fluorescent lamp (2) Sample (3) Transparent plate (Acrylic) (4) Poles (5) Rotating plate (6) Static base

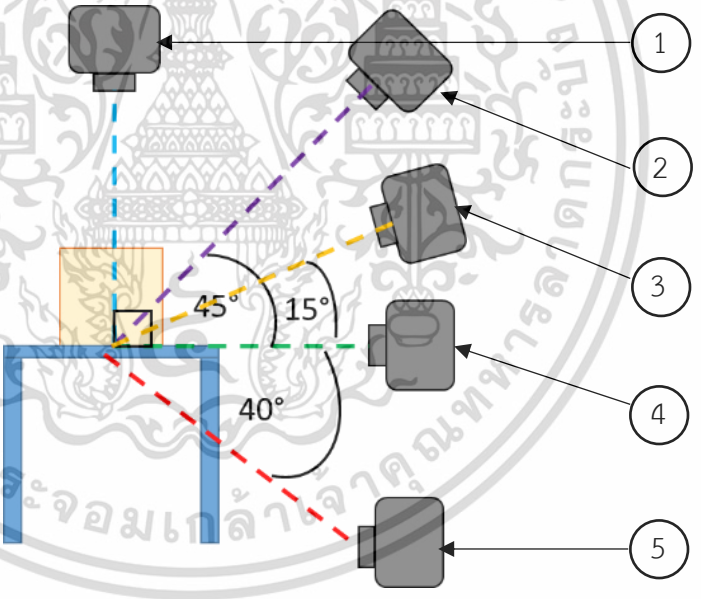

Figure 3.2 Suitable camera positions

3.3 Image Analysis

In the case of 2D image analysis (Figure 3.3), the first analysis step involved foreign object elimination from the acquired image, which was done by MATLAB® (version R2014b and 2016b, MathWork Inc., MA). Each image was cropped to 512 pixel × 512 pixel (without distortion of shape). Image segmentation was then performed by converting an RGB image into a binary image using Otsu's thresholding method.

Edge detection and holes filling were subsequently performed to extract an area of interest (AOI). Various parameters including projected area, perimeter, length in many axes, equivalent diameter, Feret's statistical diameter, form factor, roundness, extent, circularity, solidity, convexity, eccentricity, ratio, entirety, elongation, rectangularity and fractal dimension (using box counting method) were extracted from AOI. All parameters were calculated using Equations 2.3 to 2.28 (see Section 2.2.4.2).

In the case of 3D image analysis (Figure 3.3), after a 3D image was reconstructed, the image was converted into an STL file and imported into COMSOL Multiphysics® version 3.5 (COMSOL AB, Sweden) to calculate the various parameters including volume, surface area, sphericity, Wadell's roundness, radius ratio and Hoffmann shape entropy using Equations 2.30 to 2.35 (see Section 2.2.6.2).

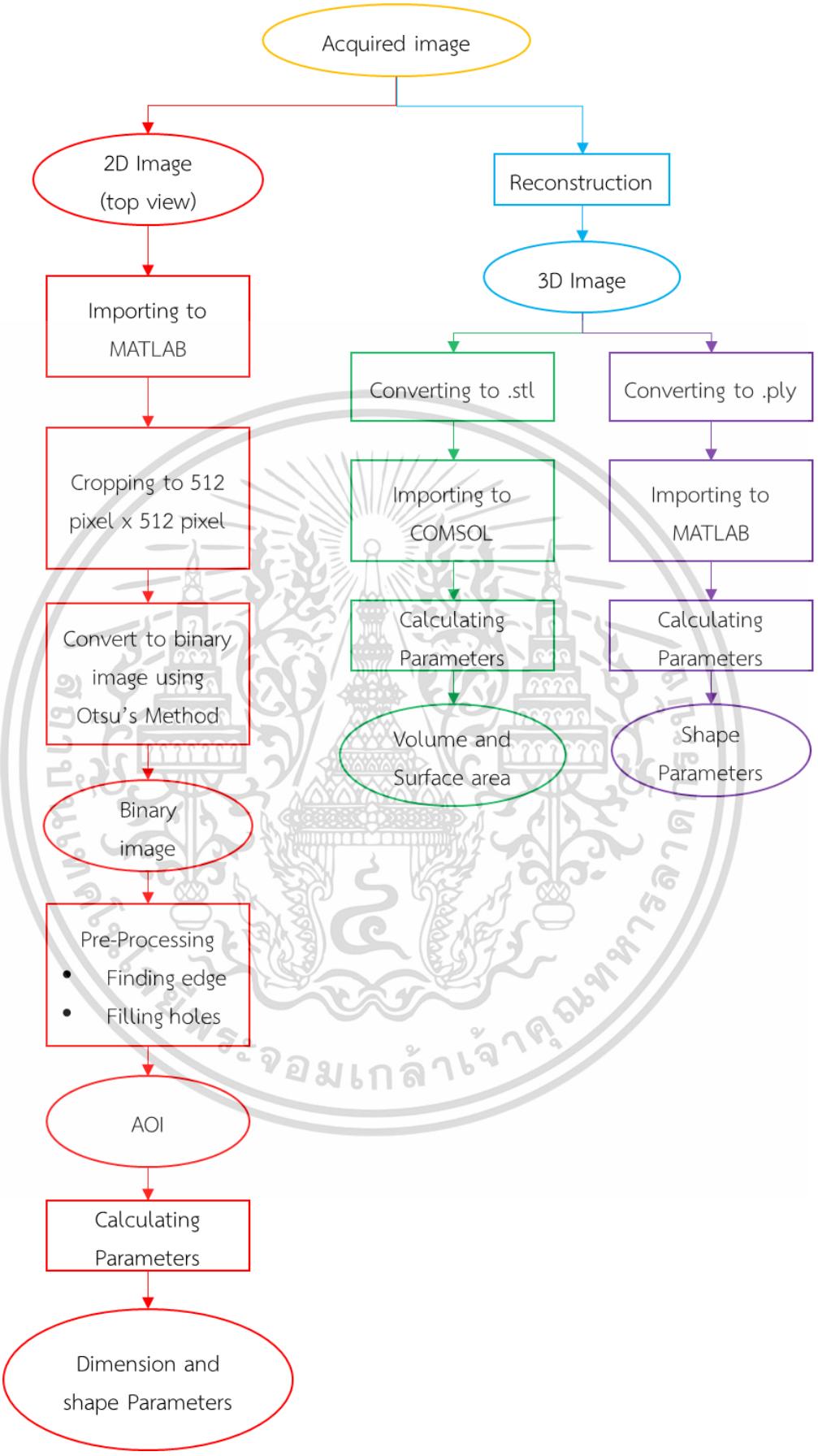

Figure 3.3 Flow chart illustrating image analysis steps

3.4 Validation of 3D Reconstructed Images

The accuracy of the image reconstruction algorithms was verified by applying such algorithms to selected standard shapes, i.e., cube, cylinder, cone and sphere (with the dimensions varied from 10 to 25 mm as shown in Table 3.1).

Comparison of the obtained image-based results was made with the results obtained from the conventional methods, i.e., use of Equations 3.1 to 3.4 to calculate the volume and liquid displacement method and Equations 3.5 to 3.8 to calculate the surface area. Various dimensions that are needed for Equations 3.1 to 3.8 were directly obtained by measurement using a venier caliper (Mitutoyo, Japan) with an accuracy of ± 0.002 mm. Information pertaining to a 3D image (i.e., volume and surface area), which was reconstructed via the developed algorithms, was also compared with that obtained from conventional 3D measurement techniques, i.e., laser scanning via a commercial scanner (Artec 3D, Artec Eva, Luxembourg).

Volume of cube $$V_c = D_1 \times D_2 \times D_3 \quad (3.1)$$

Volume of cylinder $$V_c = \pi \left(\frac{D}{2}\right)^2 h \quad (3.2)$$

Volume of cone $$V_c = \frac{\pi}{3}\left(\frac{D}{2}\right)^2 h \quad (3.3)$$

Volume of sphere $$V_c = \frac{4}{3}\pi \left(\frac{D}{2}\right)^3 \quad (3.4)$$

Surface area of cube $$SA_c = 2(D_1D_2) + 2(D_1D_3) + 2(D_2D_3) \quad (3.5)$$

Surface area of cylinder $$SA_c = 2\pi \left(\frac{D}{2}\right)^2 + \frac{\pi Dh}{2} \quad (3.6)$$

Surface area of cone $$SA_c = \pi \left(\frac{D}{2}\right)^2 + \frac{\pi D}{2}\sqrt{h^2 + \left(\frac{D}{2}\right)^2} \quad (3.7)$$

Surface area of sphere $$SA_c = 4\pi\left(\frac{D}{2}\right)^2 \quad (3.8)$$

Table 3.1 Size and dimensions of standard shapes as measured by vernier calliper

Shape	Dimension (mm)
Cube	10.30 ± 0.05
	15.32 ± 0.04
	20.06 ± 0.20
	25.21 ± 0.07
	30.21 ± 0.08
Cylinder	*D* = 10.20 ± 0.00, *H* = 10.23 ± 0.02
	D = 15.28 ± 0.03, *H* = 15.26 ± 0.03
	D = 20.25 ± 0.03, *H* = 20.40 ± 0.02
Cone	*D* = 10.11 ± 0.02, *H* = 10.19 ± 0.01
	D = 15.08 ± 0.02, *H* = 15.00 ± 0.00
	D = 20.25 ± 0.08, *H* = 20.33 ± 0.03
Sphere	*D* = 9.55 ± 0.03
	D = 16.31 ± 0.06
	D = 19.74 ± 0.03

3.5 Drying Step

Drying experiments were conducted in a convective hot air dryer (Memmert GmbH+Co. KG, UM500, Germany) at two different drying temperatures (60 °C and 80 °C). The drying air velocity was maintained at ≈ 0.1 m/s. Three cubes were taken at each predetermined drying time (every 1 h until moisture content was lower than 0.1% (d.b.)). The cubes were weighed, and their images taken. The volume of the cubes was also determined (see Section 3.7).

3.6 Moisture Content Determination

Sample was weighed using a 4-digit digital balance with an accuracy of ± 0.0002 g (Sartorius Lab Instruments GmbH+Co. KG, BSA224S-CW, Germany) and then dried in a hot air oven (Memmert GmbH+Co. KG, UM500, Germany) at 105 °C ± 2 °C until constant mass was obtained as per the AOAC method 984.25 (2000). The moisture content (MC) and moisture ratio of the sample was then calculated as per Equations 3.9 and 3.10, respectively.

$$\mathrm{MC}\ (\%\ \mathrm{d.b.}) = \frac{m - m_{\mathrm{bd}}}{m_{\mathrm{bd}}} \times 100 \quad (3.9)$$

$$\mathrm{MR} = \frac{\mathrm{MC} - \mathrm{MC_{eq}}}{\mathrm{MC_0} - \mathrm{MC_{eq}}} \tag{3.10}$$

3.7 Volume Determination

Volume of a sample was determined using a liquid displacement method with 25 mL Hubbard-Carmick specific gravity bottle (Corning, USA) and 95% n-heptane (RCI Labscan, Thailand, AR grade, density ≈ 0.680 g/cm^3) as the working liquid (Sansiribhan et al. 2010). The volume of the sample was calculated as per Equation 3.11

$$V_{\mathrm{l}} = \frac{m - m_s}{\rho} \tag{3.11}$$

3.8 Statistical Analysis

The experiments were performed at least in duplicate. The results based on the experimental data were calculated and are reported as average (Equation 3.12) and standard deviation (SD) (Equation 3.13) [32]. Differences between the results obtained via the traditional method and developed algorithms were calculated using Equations 3.14 and 3.15.

$$\bar{x} = \frac{\sum_{i=1}^{n} x_i}{n} \tag{3.12}$$

$$\mathrm{SD} = \sqrt{\frac{\sum_{i=1}^{n} (x_i - \bar{x})}{n}} \tag{3.13}$$

$$\%\ \mathrm{Difference} = \frac{V_{\mathrm{3D}} - V_{\mathrm{l}}}{V_{\mathrm{l}}} \times 100 \tag{3.14}$$

$$\%\ \mathrm{Difference} = \frac{SA_{\mathrm{3D}} - SA_{\mathrm{C}}}{SA_{\mathrm{C}}} \times 100 \tag{3.15}$$

CHAPTER 4
RESULTS AND DISCUSSION

4.1 Development of Procedures to Analyze Changes during Drying

4.1.1 Determination of Suitable Camera Position

Since 3D image need to be reconstructed from 2D images, extracting AOI from 2D images was a very important process that must be carefully performed. Agisoft LLC [33] suggested that 2D images from side and top views are appropriate 3D image reconstruction. However, such a setting implies that one cannot isolate AOI from the sample. For this reason, images should be acquired from the different angles. Based on the preliminary study, camera positions of 15°, 40° and 45° (see Figure 3.2) gave the best results as can be seen in Figure 4.1 (a).

(a) (b)

Figure 4.1 Reconstructed 3D image. (a) isolated; (b) not isolated

4.1.2 Testing of 3D Image Reconstruction Software

Preliminary experiments were also conducted to determine which image reconstruction software would give the best reconstruction result. Various software, i.e., Autodesk Recap 360 (Autodesk Inc., San Rafael, CA), Autodesk 123D Catch (Autodesk Inc., San Rafael, CA), Agisoft Photoscan (Agisoft, LLC, St. Petersburg, Russia) and Visual SFM (http://ccwu.me/vsfm/), were tested. The programs were tested by reconstructing a 3D image from the same batch of 2D images. Results suggested that Autodesk Recap 360 was the most suitable software as it gave the reconstructed image that resembled the sample the most (as observed by visual inspection) as shown in Figure 4.2.

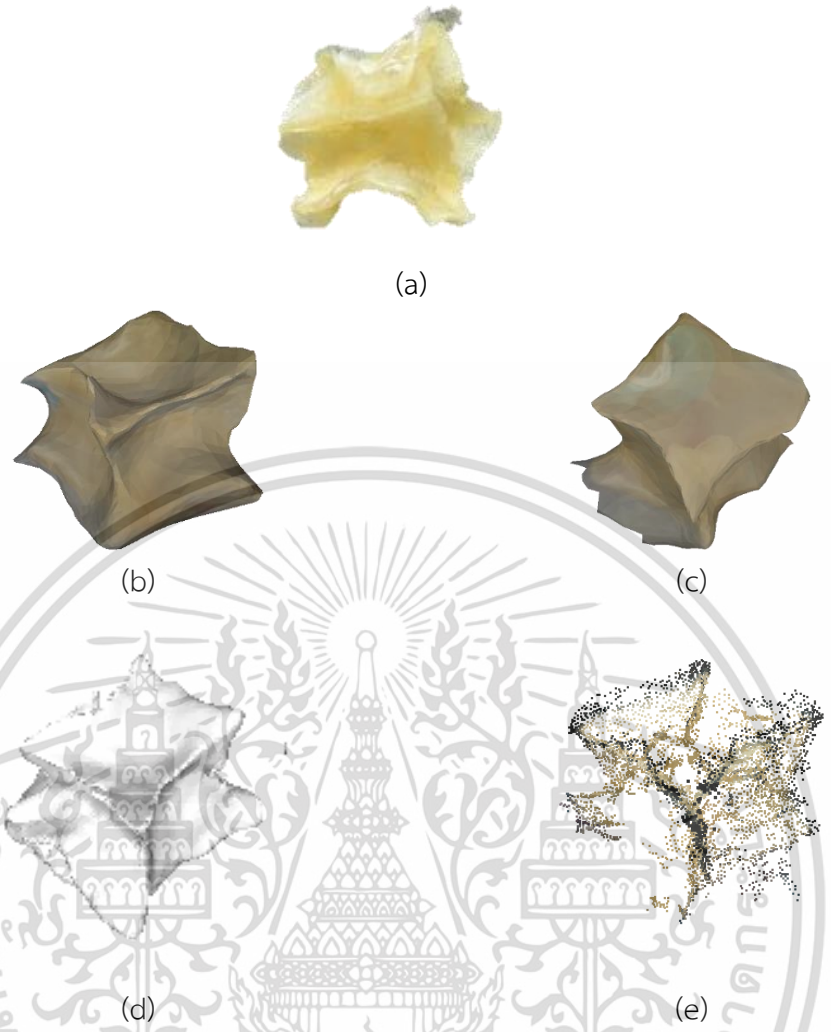

Figure 4.2 3D image reconstructed from 2D images. (a) Original image of the sample; (b) image from Autodesk Recap 360; (c) image from Autodesk 123D Catch; (d) image from Agisoft Photoscan and (e) image from Visual SFM

4.1.3 Determination of Suitable Image Acquisition Angle

Suitable image acquisition angle of the rotating platform was determined by acquiring the images of the standard shapes, i.e., cube (10 mm x 10 mm x 10 mm), cone (10 mm diameter and 10 mm height), and sphere (10 mm diameter) every 10°, 20° and 30°. Volume and surface area of the reconstructed 3D images were compared with the volume from the liquid displacement method and surface area calculated using Equations 3.5, 3.6 and 3.8. 3D images obtained at every 20° had the lowest differences in both volume and surface area from those of the original sample (Table 4.1).

Table 4.1 Comparison between volume obtained from image reconstruction and liquid displacement method as well as surface area from image reconstruction and calculation method

	Volume difference (%)			Surface area difference (%)		
	10°	20°	30°	10°	20°	30°
Cube	17.747	3.560	46.098	15.900	0.723	27.245
Cone	33.740	0.550	320.595	26.171	0.791	39.177
Sphere	10.534	9.809	19.799	17.560	14.144	41.146

4.1.4 Determination of Suitable Image Resolution

Reconstructed 3D image (from the 2D images of 10-mm cube) of different resolutions, i.e., 640 pixel x 480 pixel, 1600 pixel x 1200 pixel, 2816 pixel x 2112 pixel and 4000 pixel x 3000 pixel were compared. Reconstructed 3D images obtained from images of 640 pixel x 480 pixel and 4000 pixel x 3000 pixel were distorted due to lacks of detail (lack of points to stitched the images together) and excessive information (too many points of both objects and background, so the wrong points were stitched together), respectively. On the other hand, both images of 1600 pixel x 1200 pixel and 2816 pixel x 2112 pixel resulted in well stitched 3D images with nearly identical results. Therefore, 1600 pixel x 1200 pixel was chosen due to the faster processing time and less required storage space.

(a) (b) (c)

Figure 4.3 3D image reconstructed from 2D images of the different resolutions. (a) 1600 pixel x 1200 pixel; (b) 2816 pixel x 2112 pixel and (c) 4000 pixel x 3000 pixel

4.1.5 Determination of Suitable Camera Parameters

Results of the process to determine suitable camera parameters, i.e., aperture, ISO and shutter speed are shown in Figure 4.4. Appropriate parameters were noted to be those that resulted in an image that was not too bright (Figures 4.4 (a) and 4.4 (b))

or too dark (Figures 4.4 (e) and 4.4 (f)) since these would provide inadequate information of a sample. The appropriate images are shown in Figures 4.4 (c) and 4.4 (d). The appropriate ranges for aperture, ISO and shutter speed were 2.8 to 8.0, 100 to 400 and 1/125 s to 1/500 s, respectively. Reconstructed 3D images from the appropriate setting parameters are shown in Figure 4.5 (a); the green dots present finished reconstructed 3D image (Figure 4.5 (b)). Image-based volume and surface area were then compared with the results from the calculation using 10-mm cube, 10-mm diameter cone and 10-mm diameter sphere as the reference samples. Aperture = 8, ISO = 200 and shutter speed = 1/125 s yielded the differences of less than 10%, except in the case of the surface area of sphere (Table 4.2). The reason is that although the surface area of sphere was coated by white matte spray, the surface was still glossy resulting in poor image acquisition. The algorithms interpreted both the light and dark points as the convex and concave and hence the distorted 3D images.

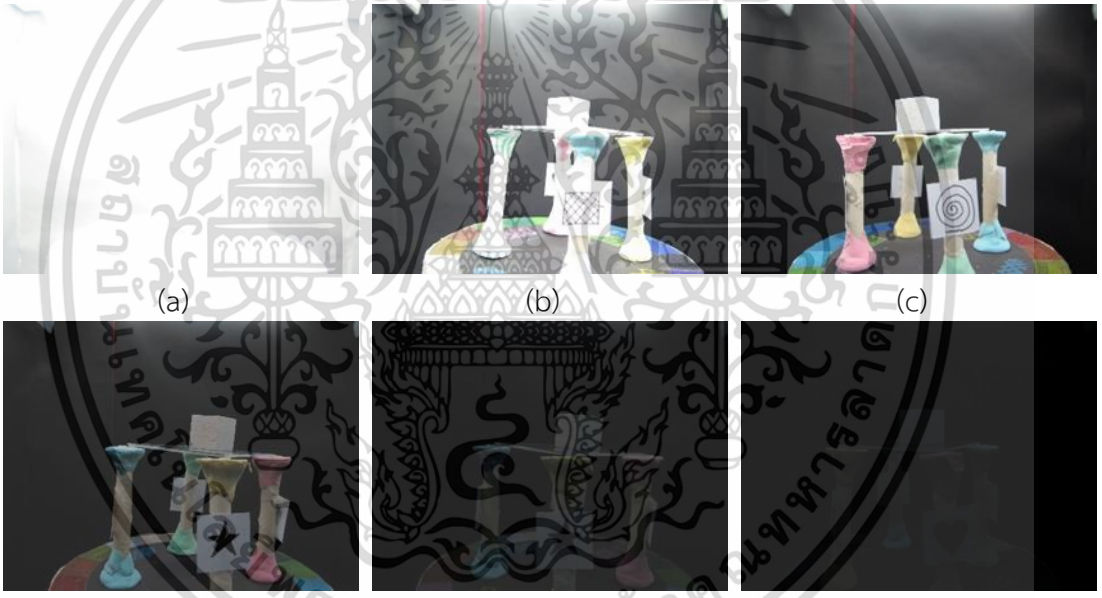

Figure 4.4 Images of a cube acquired by using aperture/ ISO/ shutter speed of (a) 2/ 100/ 1/30 s; (b) 2/ 400/ 1/125 s; (c) 2/ 100/ 1/125 s; (d) 8/ 400/ 1/125 s; (e) 8/ 200/ 1/125 s; (f) 8/ 100/ 1/500 s

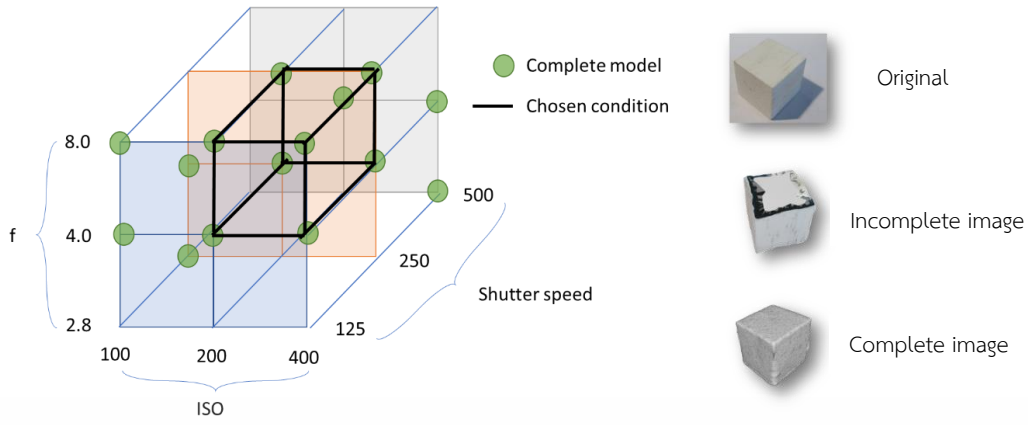

(a) (b)

Figure 4.5 Result of 3D image reconstruction using various camera parameters. (a) Chosen conditions; (b) original images, incomplete 3D and complete 3D images

Table 4.2 Comparison between image-based volume and surface area of various shapes and volume obtained from liquid displacement method and surface area by calculation

Condition			Volume difference (%)			Surface area difference (%)			
Aperture	Shutter speed	ISO	Cube	Cone	Sphere	Cube	Cone	Sphere	Cube
4.0	1/125	200	9.953	42.278	13.850	3.276	30.553	8.681	3.276
		400	6.602	16.434	35.755	7.878	16.421	9.943	7.878
	1/250	200	30.268	44.051	9.549	17.717	28.061	11.754	17.717
		400	25.593	53.777	6.977	16.268	31.910	13.715	16.268
5.6	1/125	200	4.004	33.243	16.532	0.036	22.037	6.050	0.036
		400	N/A	48.106	2.844	N/A	29.817	18.651	N/A
	1/250	200	12.538	25.833	11.983	6.416	16.851	12.749	6.416
		400	13.530	45.380	8.275	7.984	28.358	13.133	7.984
8	1/125	200	3.560	23.850	9.809	4.777	12.666	9.201	4.777
		400	22.868	33.910	10.692	13.853	26.528	13.404	13.853
	1/250	200	3.560	0.550	9.809	0.723	0.791	14.144	0.723
		400	15.068	1.519	33.222	8.985	7.005	3.830	8.985

4.2 Validation of Reconstructed 3D Images

Volume of the reconstructed 3D images of the standard (reference) shapes were converted from voxel to mm^3. Relationships between the image-based volume and that obtained from liquid displacement are shown in Figures 4.6 to 4.10; the relationships are given by Equations 4.1 to 4.4.

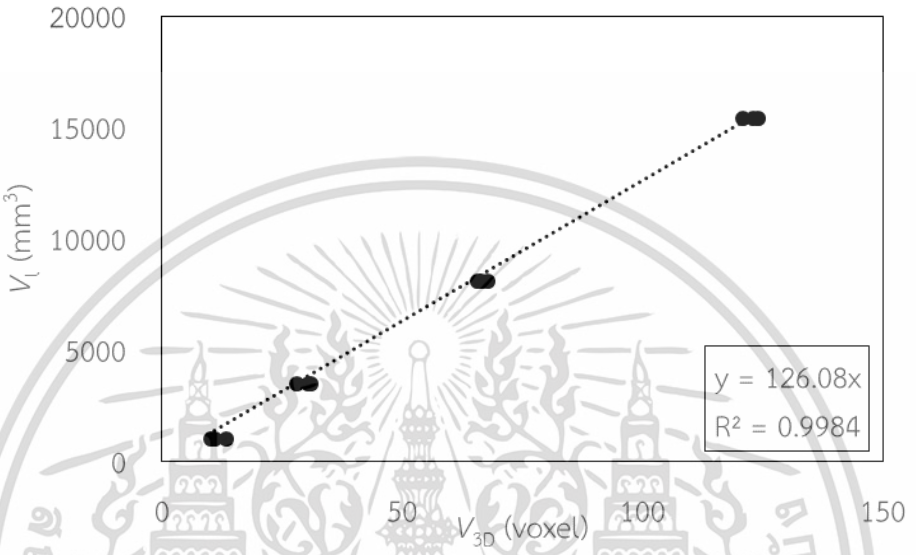

Figure 4.6 Relationship between volume of 3D image (V_{3D}) and volume obtained via liquid displacement (V_l) of the cube

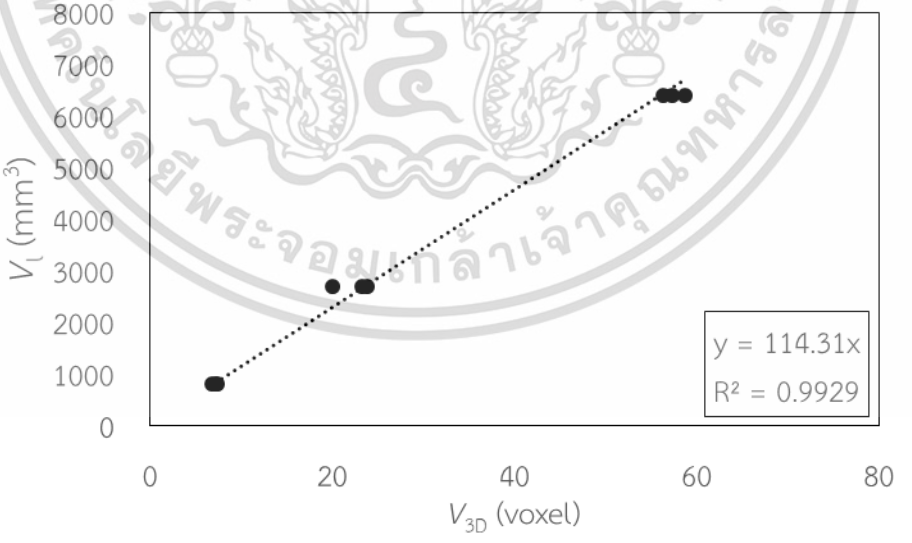

Figure 4.7 Relationship between volume of 3D image (V_{3D}) and volume obtained via liquid displacement (V_l) of the cylinder

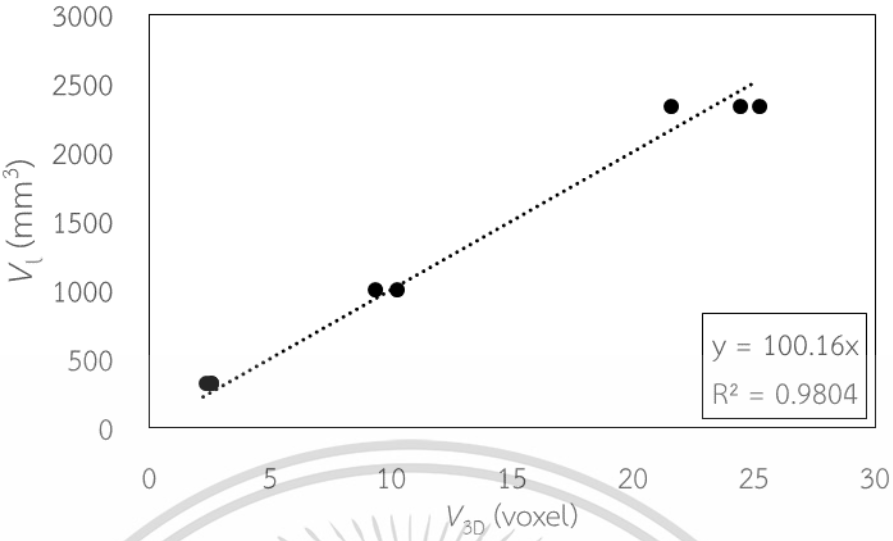

Figure 4.8 Relationship between volume of 3D image (V_{3D}) and volume obtained via liquid displacement (V_l) of the cone

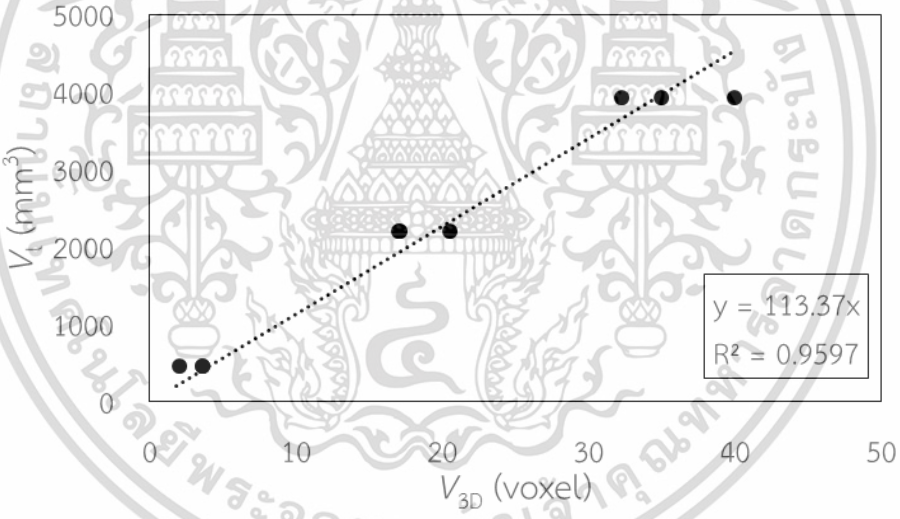

Figure 4.9 Relationship between volume of 3D image (V_{3D}) and volume obtained via liquid displacement (V_l) of the sphere

Cube $$V_{\mathrm{l}} = 126.08V_{\mathrm{3D}} \quad (4.1)$$

Cylinder $$V_{\mathrm{l}} = 114.31V_{\mathrm{3D}} \quad (4.2)$$

Cone $$V_{\mathrm{l}} = 100.16V_{\mathrm{3D}} \quad (4.3)$$

Sphere $$V_{\mathrm{l}} = 113.37V_{\mathrm{3D}} \quad (4.4)$$

Table 4.3 and Figure 4.10 show the differences in the volume of standard shapes as obtained by different measurement methods. Sizes between 15 mm to 25 mm were selected. If the sizes of the objects were smaller than the selected sizes, the algorithms could not capture the detail of the objects. In contrast, if the size of the objects were larger than the selected sizes, the algorithms connected the objects and the base together. Note that the volumes of the reconstructed 3D images in all cases were no more than 10% different from the values obtained using liquid displacement method. Therefore, the reconstruction process was adequate.

Table 4.3 Comparison between volumes obtained from liquid displacement, laser scanning, calculation and image reconstruction methods

Shape	Volume (mm^3)						
	Liquid displacement	Laser scanning		Calculation		Image reconstruction	
	Value	Value*	% Difference	Value	% Difference	Value	% Difference
Cube	1121.687 ± 3.926 (0.350%)	998.500	5.878	1091.293 ± 6.457 (0.592%)	2.869	1373.726 ± 214.154 (15.589%)	22.470
	3584.157 ± 23.662 (0.660%)	3550.000	0.757	3595.639 ± 16.264 (0.452%)	2.052	3684.058 ± 191.206 (5.190%)	2.787
	8227.685 ± 335.320* (4.076%)	8096.000	1.601	8069.858 ± 50.530 (0.626%)	1.918	8330.946 ± 143.877 (1.727%)	1.255
	15506.783 ± 297.389* (1.918%)	15530.000	0.150	16015.294 ± 55.319 (0.345%)	3.281	15398.571 ± 203.819 (1.324%)	0.698
	26720.194 ± 401.700** (1.503%)	27110.000	4.925	27561.607 ± 54.813 (0.199%)	6.673	N/A	N/A
Cylinder	870.445 ± 15.009 (1.724%)	787.200	2.768	835.650 ± 1.887 (0.226%)	3.216	781.156 ± 34.675 (4.439%)	10.258
	2744.375 ± 22.322 (0.813%)	2560.000	6.718	2798.299 ± 16.780 (0.600%)	1.965	2523.203 ± 230.335 (9.129%)	8.059
	6441.789 ± 77.726 (1.207%)	6075.000	5.694	6572.247 ± 18.725 (0.285%)	2.025	6400.149 ± 141.118 (2.161%)	1.372

Table 4.4 Comparison between volumes obtained from liquid displacement, laser scanning, calculation and image reconstruction methods (cont'd)

Shape	Volume (mm^3)						
	Liquid displacement	Laser scanning		Calculation		Image reconstruction	
	Value	Value*	% Difference	Value	% Difference	Value	% Difference
Cone	348.178 ± 18.312 (5.260%)	322.100	12.095	272.766 ± 1.124 (0.412%)	5.074	238.815 ± 12.174 (5.098%)	31.410
	1026.730 ± 7.710 (0.751%)	978.500	1.305	893.024 ± 2.369 (0.265%)	7.545	969.849 ± 64.733 (6.675%)	5.540
	2352.180 ± 13.786 (0.586%)	2270.000	0.932	2182.90.6 ± 19.575 (0.897%)	4.733	2367.782 ± 192.138 (8.115%)	0.663
Sphere	486.658 ± 8.261 (1.697%)	454.900	6.828	456.533 ± 4.375 (0.958%)	7.211	327.866 ± 103.092 (31.443%)	32.629
	2240.407 ± 29.785 (1.329%)	2234.000	0.286	2273.200 ± 24.184 (1.064%)	1.464	2041.038 ± 224.519 (11.000%)	8.899
	3958.053 ± 88.282 (2.230%)	3988.000	0.757	4027.567 ± 21.225 (0.527%)	1.756	4029.170 ± 445.117 (11.047%)	1.797

Note: *Percent differences were calculated in comparison with the values obtained via liquid displacement. Laser scanning was performed only in single replication.

** Sample size was larger than the utilized Hubbard-Carmick specific gravity bottle, so the 50-ml beaker was used instead.

*** The values in brackets are percent SD.

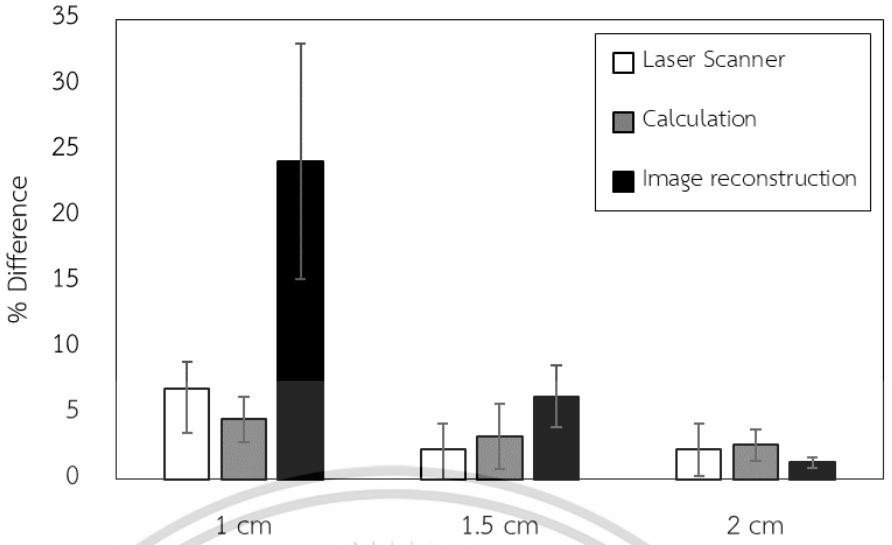

Figure 4.10 Difference in volume as obtained via different method

4.3 Changes Occurred during Drying

Image-based parameters were determined and used to monitor non-uniform deformation. Figure 4.11 shows that the change in volume followed the change in moisture content because when water evaporated, the structure of the gel collapsed, hence the decreasing in the volume. On the other hand, the decrease in the volume did not agree with the change in shape as shown in Figure 4.12. From the beginning until 2 h of drying, shape change did not take place, while the volume continuously decreased. After 6 h, shape started to change as well.

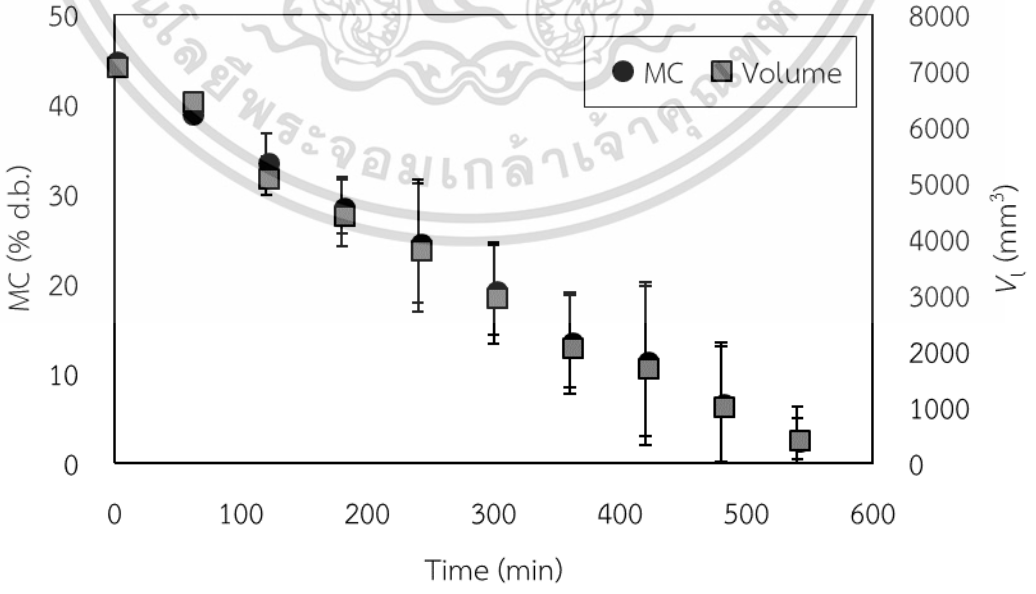

Figure 4.11 Moisture content (dry basis) and volume of 2% agar gel (0% sugar) during drying at 80 °C

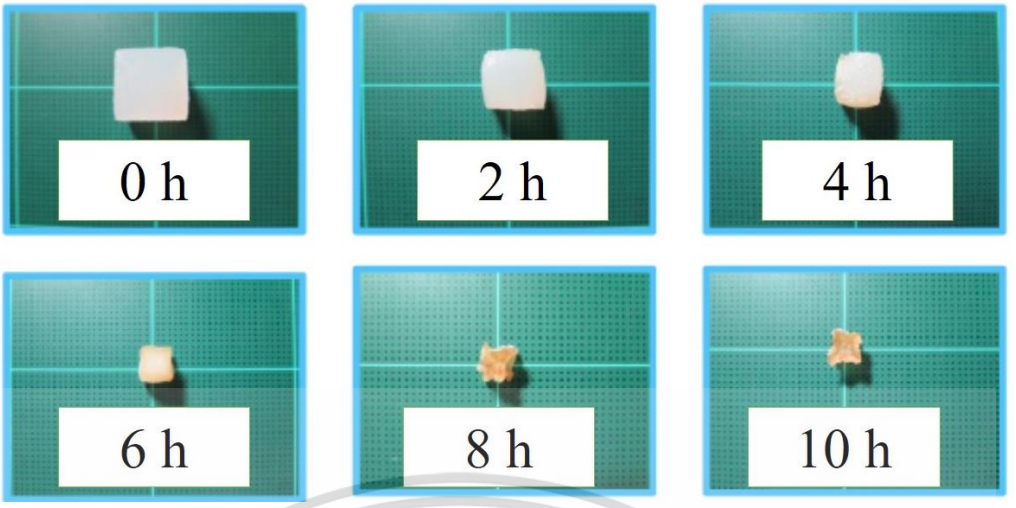

Figure 4.12 Deformation of agar gel (0% sugar) during drying at 80 °C

4.3.1 Changes in 2D Image-Based Parameters

Figures 4.13 to 4.20 show the changes in the 2D image-based parameters (in groups of similar types) as a function of the moisture ratio. Some parameters, i.e., projected area, perimeter, square-circularity and area/perimeter decreased upon drying (see Figures 4.13, 4.14 and 4.16) as a result of the material shrinkage. $Extent_{box}$ and $Rectangularity_{ef}$ (see Figures 4.17 and 4.18) exhibited the same trend. SD radius and fractal dimension, which are shown in Figures 4.19 and 4.20, also exhibited the same trend of change.

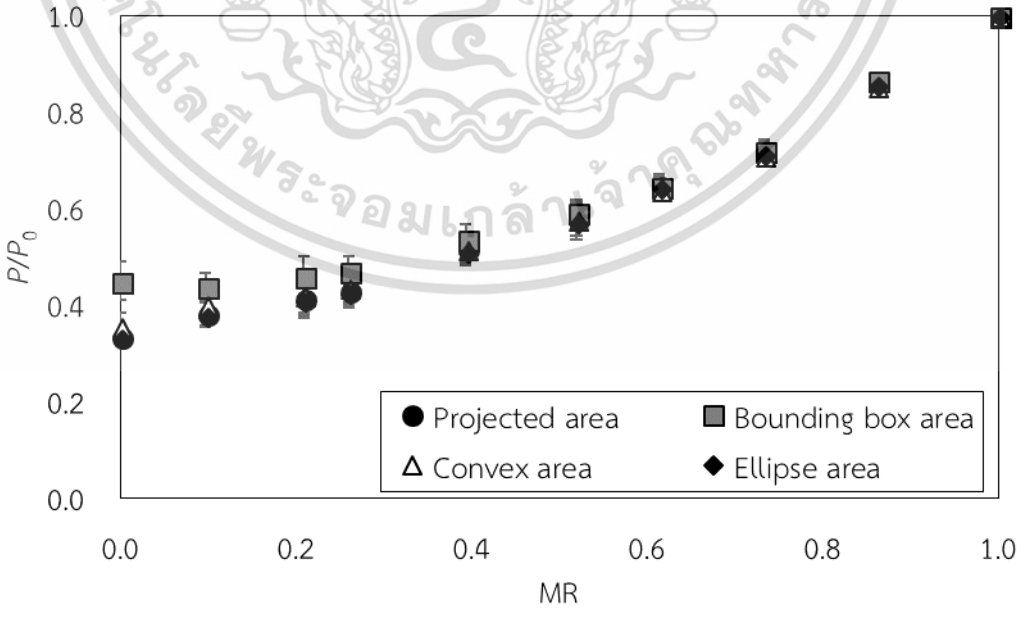

Figure 4.13 Changes in 2D parameters (area group) as a function of moisture ratio of agar gel (0% sugar) during drying at 80 °C

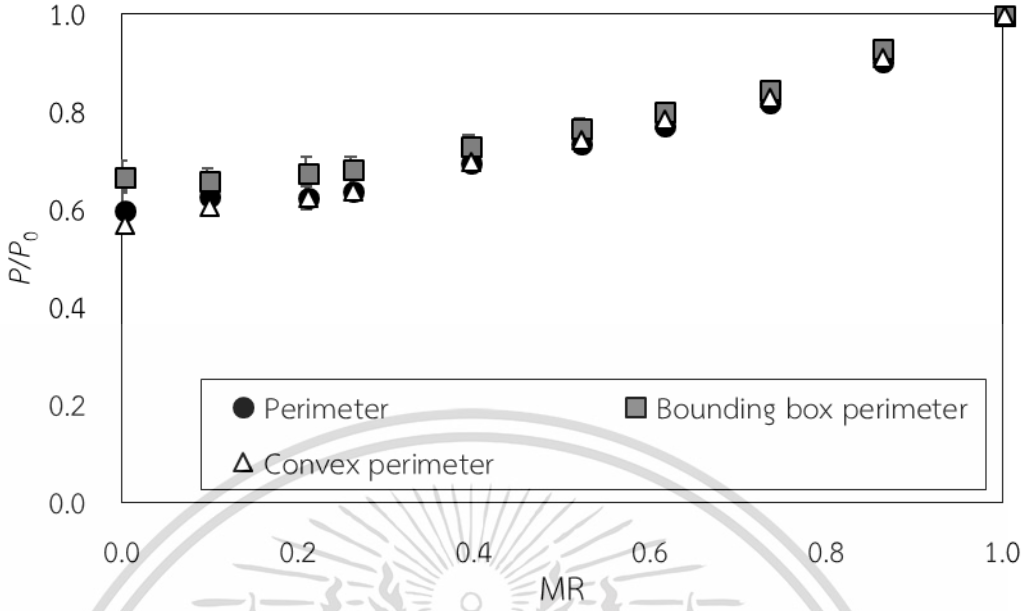

Figure 4.14 Changes in 2D parameters (perimeter group) as a function of moisture ratio of agar gel (0% sugar) during drying at 80 °C

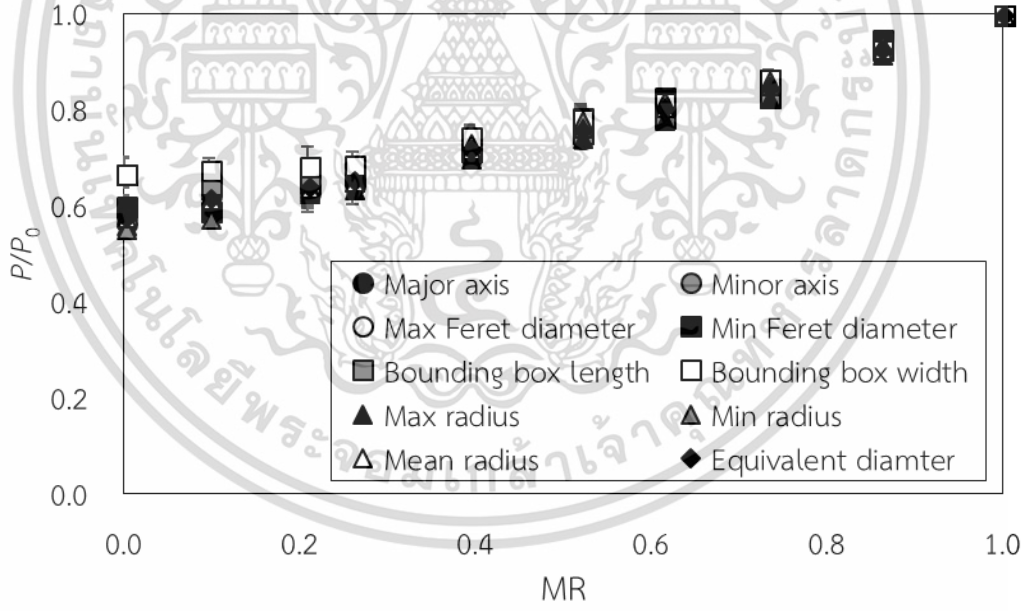

Figure 4.15 Changes in 2D parameters (length and radius group) as a function of moisture ratio of agar gel (0% sugar) during drying at 80 °C

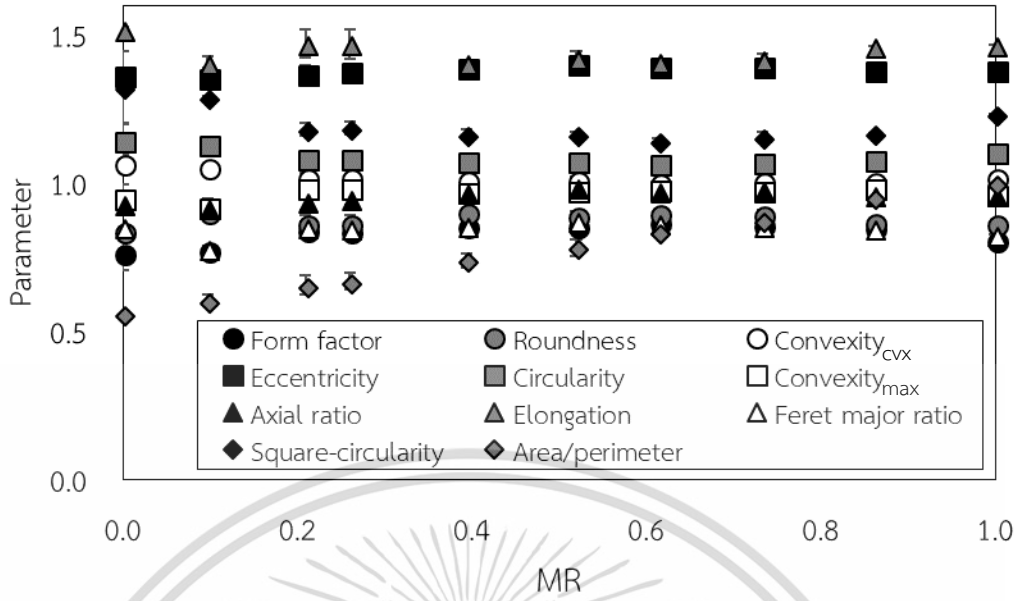

Figure 4.16 Changes in 2D parameters (circularity group) as a function of moisture ratio of agar gel (0% sugar) during drying at 80 °C

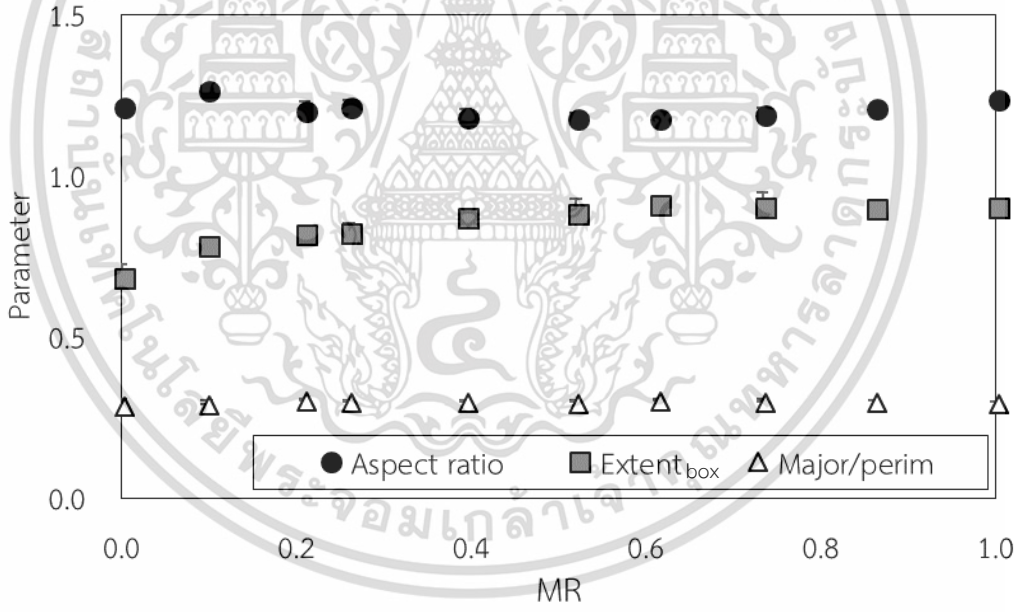

Figure 4.17 Changes in 2D parameters (stretching out group) as a function of moisture ratio of agar gel (0% sugar) during drying at 80 °C

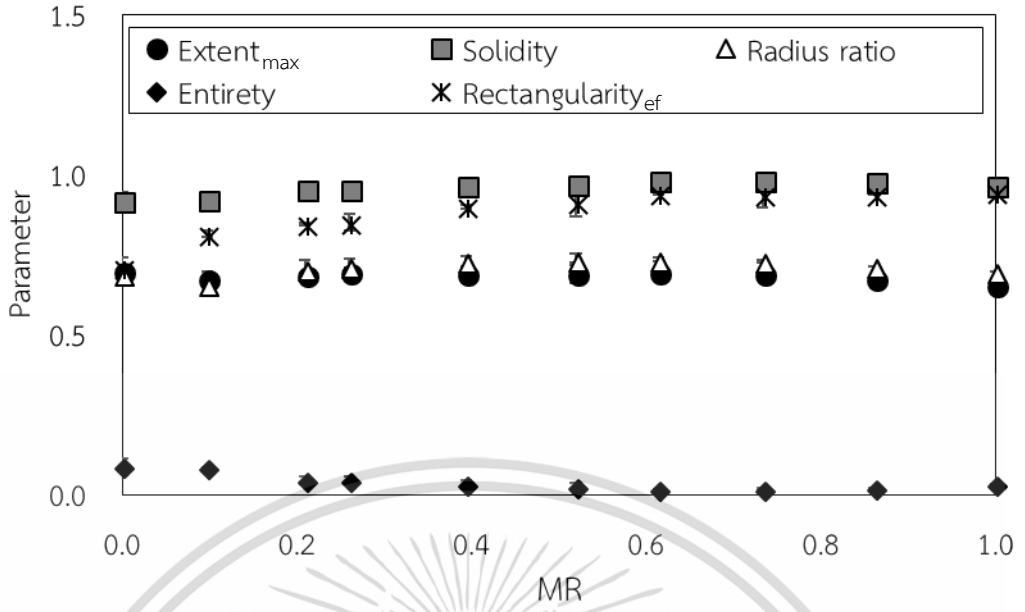

Figure 4.18 Changes in 2D parameters (filled out group) as a function of moisture ratio of agar gel (0% sugar) during drying at 80 °C

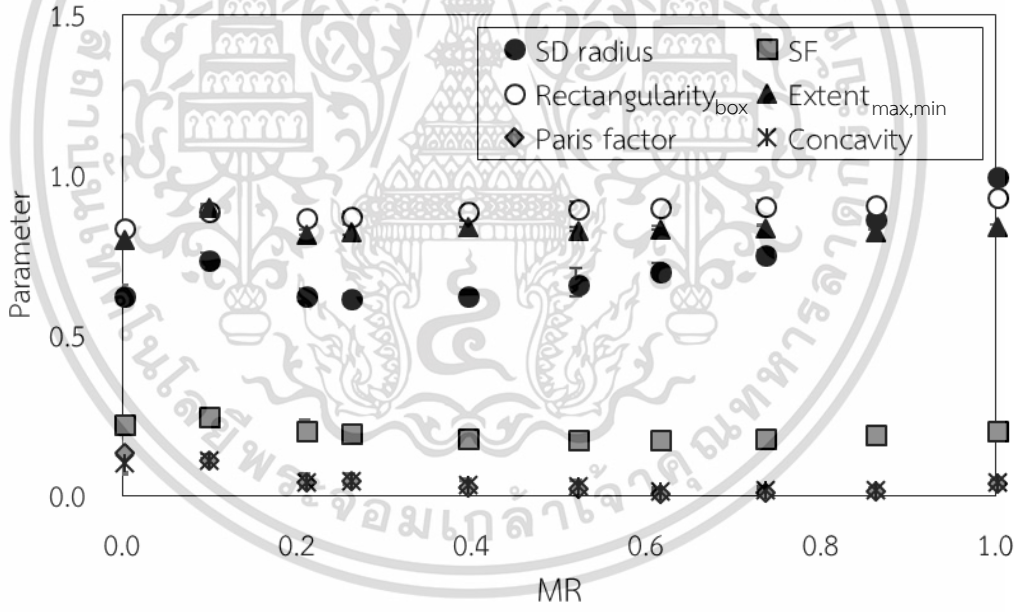

Figure 4.19 Changes in 2D parameters (edge roughness group) as a function of moisture ratio of agar gel (0% sugar) during drying at 80 °C

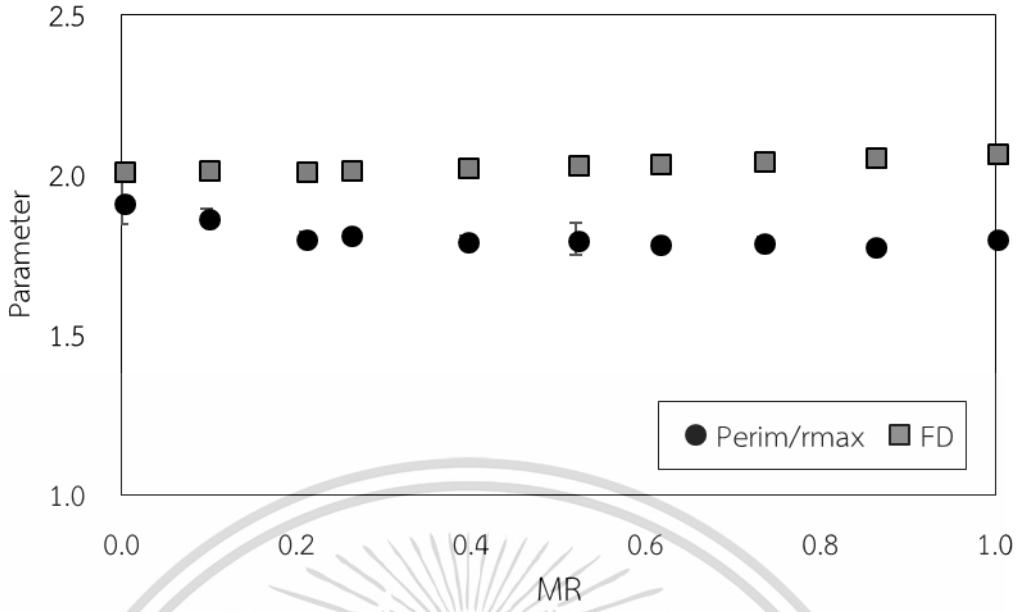

Figure 4.20 Changes in 2D parameters (edge roughness group) as a function of moisture ratio of agar gel (0% sugar) during drying at 80 °C (cont'd)

Parameters were analyzed to describe non-uniform deformation (or in other words, change of shape). It was found that only the $Extent_{box}$ and $Rectangularity_{ef}$ could be used for such a purpose. These two parameters did not significantly change until the moisture ratio was around 0.4, beyond which their values started to decrease. The results agreed well with those from visual inspection (Figure 4.21) that the sample started to experience its shape change at the moisture ratio of around 0.4. $Extent_{box}$ should be regarded as the most suitable parameter for non-uniform deformation evaluation due to its simplicity. $Extent_{box}$ decreased less than 10% from its initial value as the moisture ratio decreased from unity to the value of around 0.4.

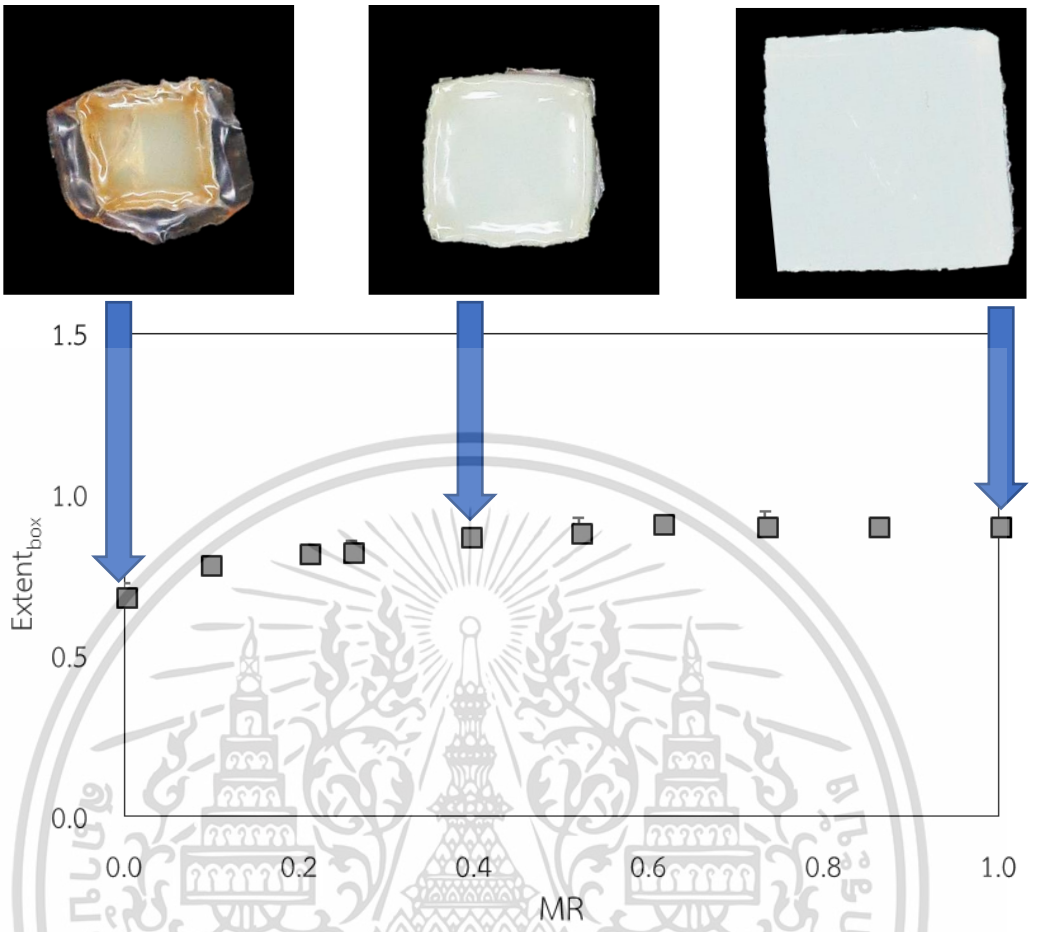

Figure 4.21 Change in Extent$_{box}$ in comparison with visually observed results

Other parameters, on the other hand, decreased right from the start of the drying process. For this reason, if non-uniform deformation is to be monitored, only Extent$_{box}$ and Rectangularity$_{ef}$ should be used. On the other hand, if only volumetric shrinkage is to be monitored, any other parameters could also be used.

4.3.2 Changes in 3D Image-Based Parameters

Figures 4.22 to 4.24 show the evolutions of the 3D image-based parameters as a function of the moisture ratio. Volume, surface area and surface area of equal sphere of the reconstructed 3D images are shown in Figure 4.22, while Figures 4.23 and 4.24 present the evolutions of the various shape parameters, i.e., sphericity, Wadell's sphericity, radius ratio, Wadell's roundness and Hoffmann shape entropy. It is seen that the general trends of the results belonging to the different spehericity factors were similar. The sphericity value should then be regarded as the most suitable parameter for non-uniform deformation evaluation due to its simplicity in much the same way as Extent$_{box}$.

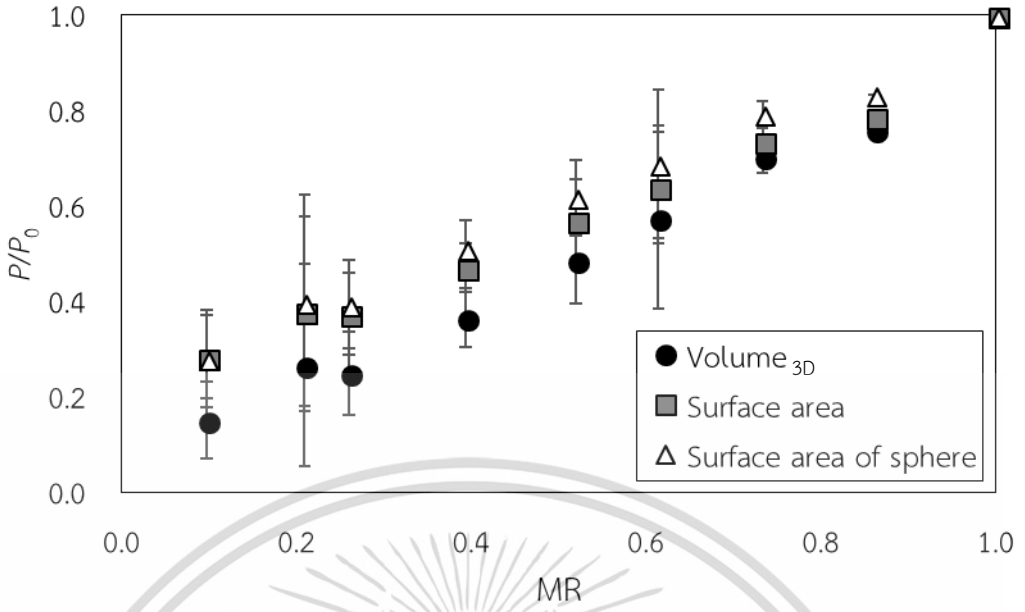

Figure 4.22 Changes in 3D parameters (dimension group) as a function of moisture ratio of agar gel (0% sugar) during drying at 80 °C

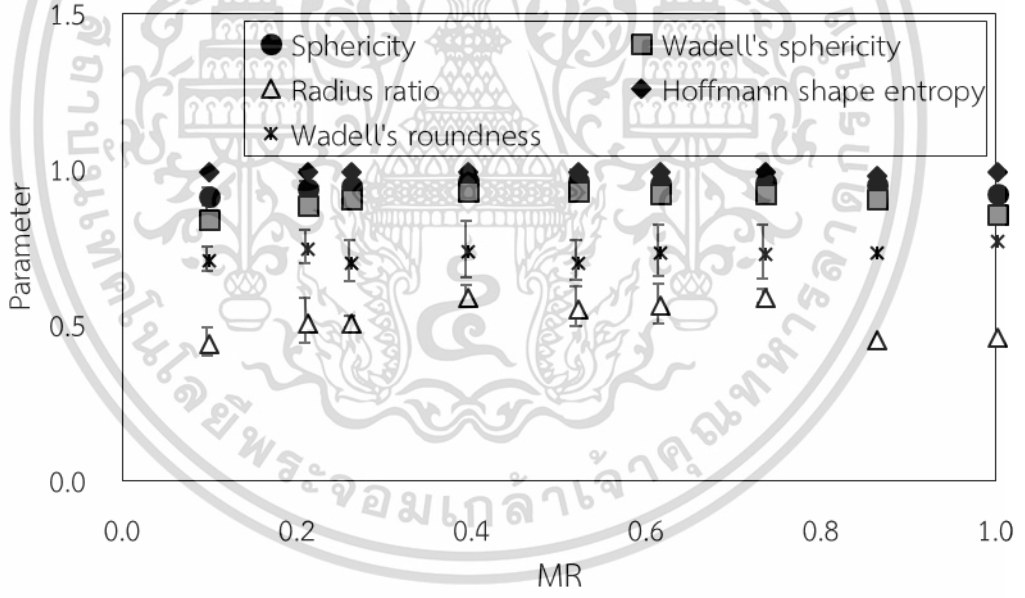

Figure 4.23 Changes in 3D parameters (shape factor group) as a function of moisture ratio of agar gel (0% sugar) during drying at 80 °C

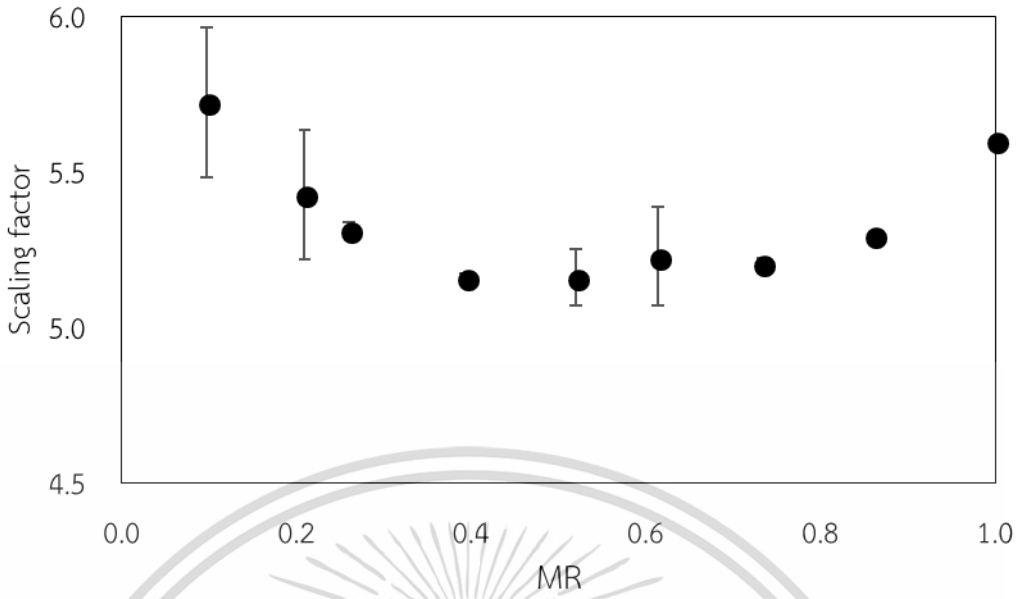

Figure 4.24 Changes in 3D parameters (scaling factor) as a function of moisture ratio of agar gel (0% sugar) during drying at 80 °C.

4.4 Effect of Drying Temperature

Drying experiments were conducted at two different temperatures, including 60 °C (slow drying rate) and 80 °C (moderate drying rate), at an air velocity around 0.1 m/s in order to study the effect of drying rate on the test material deformation. Agar gels with both 0% and 20% sugar were tested. The higher drying temperature led to a higher drying rate (see Figure 4.25), but volume changes of the drying samples at either drying temperature at the same moisture ratios were not different as can be seen in Figure 4.26. However, after prolonged drying, the samples started to deform non-uniformly as mention earlier. The point (time) when non-uniform deformation started to take place depended on the rate of drying; higher drying air temperature resulted in easier onset of the non-uniform deformation.

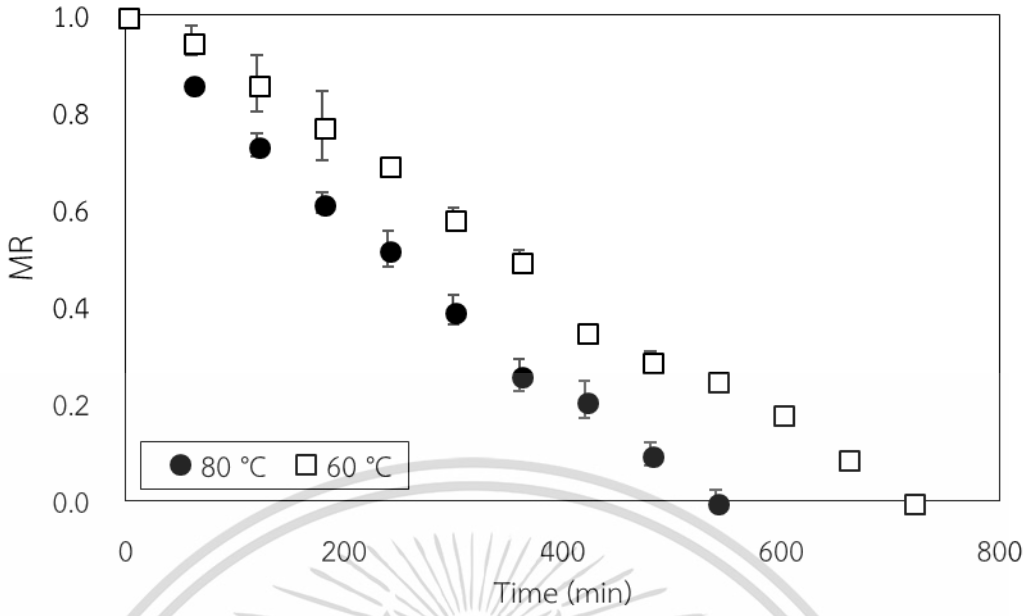

Figure 4.25 Drying curves of agar gel (0% sugar) at different drying temperatures

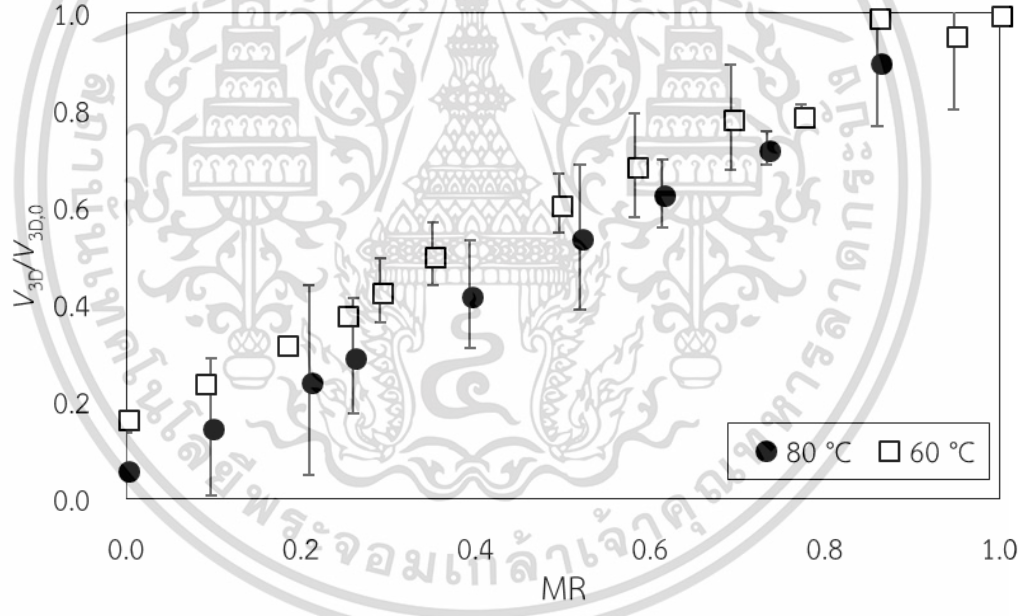

Figure 4.26 Volume ratio as a function of moisture ratio of agar gel (0% sugar)

Based on the aforementioned 2D image and 3D image analyses, $Extent_{box}$ and sphericity were chosen, respectively, to monitor the sample deformation as shown in Figure 4.27. Both $Extent_{box}$ and sphericity exhibited the same trends. This means that drying rate did not affect the deformation of the samples. Moisture change was indeed the parameter that affected the deformation as both $Extent_{box}$ and sphericity changed with the moisture ratio.

Figure 4.27 Evolutions of deformation parameters as a function of moisture ratio. Agar gel (0% sugar) was dried at different drying temperatures

4.5 Effect of Sugar Content

Drying of the gel with a higher sugar content was slower, as expected. Figure 4.28 shows the drying curves of agar gel containing different sugar contents at 80 °C. Although the initial moisture contents of agar gels with 10% and 20% sugar were significantly different from that of the gel with 0% sugar, which were 45.11% ± 0.53%, 4.89% ± 0.08% and 2.76% ± 0.16% respectively, the evolution of the volumetric shrinkage of the gels with different sugar contents as a function of the moisture ratio was similar (see Figure 4.29). For this reason, volumetric shrinkage can be used to monitor the degree of shrinkage; it cannot, however, be used to indicate the onset of non-uniform deformation.

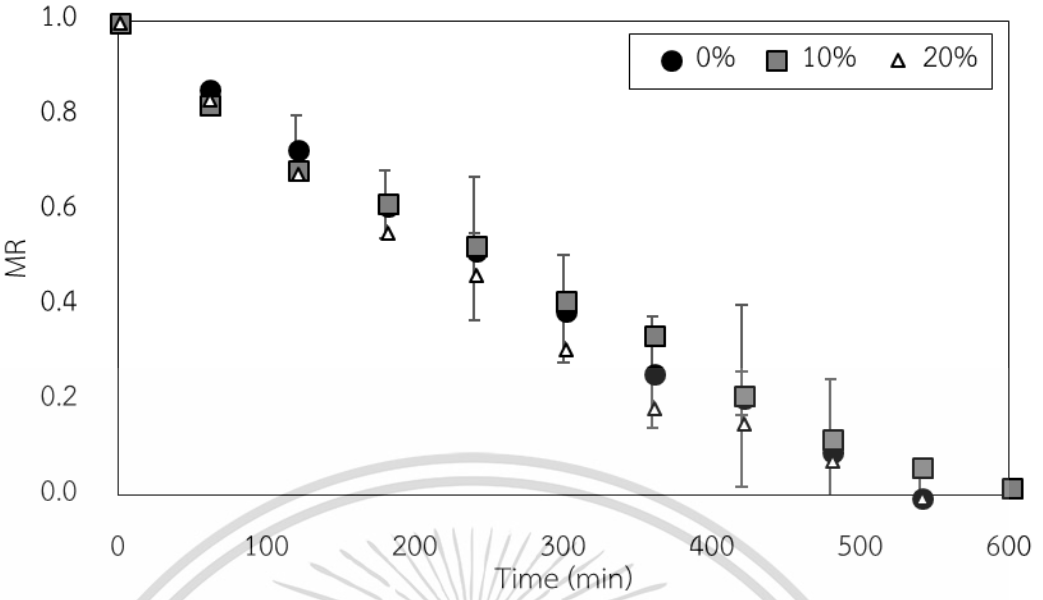

Figure 4.28 Drying curves of agar gel with different sugar contents during drying at 80 °C

Figure 4.29 Evolutions of deformation parameters as a function of moisture ratio. Agar gels with different sugar contents were dried at 80 °C

Similar observations (as mentioned earlier in Section 4.3) were noted when considering the results of other image-based parameters, which are shown in Figure 4.30. The results indicated that at moisture ratios lower than 0.4, non-uniform deformation took place. Extent$_{box}$ could be used to identify the onset and to monitor non-uniform deformation in two dimensions, while sphericity could be used for such tasks in three dimensions, regardless of the sugar content.

In the case of the gel sample with a sugar content of 20%, non-uniform deformation was not observed from the data presented in Figure 4.31. This is probably because the solids content of such a sample was high, resulting in the denser structure that could resist deformation. Drying also took place much more slowly and hence the lower level of moisture gradients that could in turn result in the non-uniform deformation. This combined effect most probably led to the absence of the non-uniform deformation in this case.

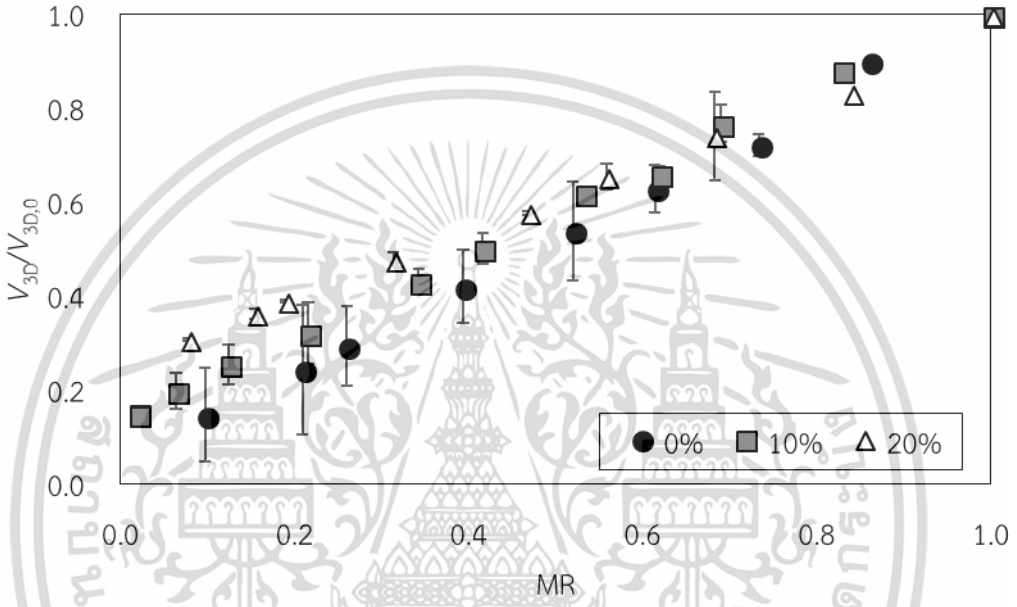

Figure 4.30 Volume ratio as a function of moisture ratio of agar gel with different sugar contents during drying at 80 °C

CHAPTER 5
CONCLUSIONS AND RECOMMENDATIONS

5.1 Conclusions

In this study, algorithms and software were developed to first reconstruct 3D images from 2D images; standard geometrical shapes, i.e., cube, cone, cylinder and sphere, were used for the validation and calibration purposes. Various parameters, both in two dimensions, i.e., projected area, perimeter, length in many axes, equivalent diameter, Feret's statistical diameter, form factor, roundness, extent, circularity, solidity, convexity, eccentricity, roundness, ratio, entirety, elongation, rectangularity and fractal dimension (using box counting method); and in three dimensions, i.e., volume, surface area, sphericity, Wadell's roundness, radius ratio and Hoffmann shape entropy, were then calculated and compared to determine the feasibility of using these parameters to monitor non-uniform deformation, which commonly takes place during drying of shrinkable materials. Agar gels with different sugar contents (0%, 10% and 20%) were used as the test materials and allowed to undergo drying at different temperatures (60 °C and 80 °C).

Difference in volume obtained via the image reconstruction and liquid displacement methods was less than 5% when the sample size was between 15 to 20 mm. The results showed that the sugar content and drying temperature did not significantly affect deformation if the various samples were assessed at the same moisture ratios. $Extent_{box}$ could describe the deformation characteristics in 2D, while sphericity could be used to describe the deformation in 3D. Despite the aforementioned capability, these parameters could only be used to indicate the period of deformation but cannot quantify the degree/level of deformation. Nevertheless, this study represents a first step for future development of a real-time and/or in situ monitoring and control system for a drying process of high-value foods and soft biomaterials via the use of a computer vision system.

5.2 Recommendations

Further study should be performed on real food materials with various shapes and sizes to confirm the feasibility of using image analysis to monitor and evaluate the deformation of shrinkable food materials.

In addition, attempts should be made to use the obtained results to develop a feedback control system to control a food processing operation (not only drying), so that a high quality product can be produced.

References

[1] Mujumdar, A.S. Editors. **Handbook of Industrial Drying**. 4th ed. Boca Raton : CRC Press. 2015.

[2] Niamnuy, C., Devahastin, S., Soponronnarit, S. and Raghavan, G.S.V. 2008. "Modeling coupled transport phenomena and mechanical deformation of shrimp during drying in a jet spouted bed dryer." **Chemical Engineering Science**. 63(22) : 5503-5512.

[3] Raghavan, G.S.V. and Silveira, A.M. 2001. "Shrinkage Characteristics of Strawberries Osmotically Dehydrated in Combination with Microwave Drying." **Drying Technology**. 19(2) : 405-414.

[4] Sansiribhan, S., Devahastin, S. and Soponronnarit, S. 2010. "Quantitative evaluation of microstructural changes and their relations with some physical characteristics of food during drying." **Journal of Food Science**. 75(7) : E453-E461.

[5] Panyawong, S. and Devahastin, S. 2007. "Determination of deformation of a food product undergoing different drying methods and conditions via evolution of a shape factor." **Journal of Food Engineering**. 78(1) : 151-161.

[6] Devahastin, S., Suvarnakata, P., Soponronnarit, S. and Mujumdar, A.S. 2004. "A comparative study of low-pressure superheated steam and vacuum drying of a heat sensitive material." **Drying Technology**. 22(8) : 1845-1867.

[7] Devahastin, S. and Niamnuy, C. 2010. "Modelling quality changes of fruits and vegetables during drying: a review." **International Journal of Food Science and Technology**. 45 : 1755-1767.

[8] Jinorose, M., Stienkijumpai, A. and Devehastin, S. 2017. "Use of Image Analysis as a Monitoring Tool for Non-Uniform Deformation of Shrinkable Materials during Drying." **Journal of Chemical Engineering.of Japan**. 50(10) : 785-791.

[9] Bullard, J.W. and Garboczi, E.J. 2013. "Defining shape measures for 3D star-shaped particles: Sphericity, roundness, and dimensions." **Powder Technology**. 249 : 241-252.

[10] Radvilaite, U., Ramirez-Gomez, A, Kacianauskas, R. 2016. "Determining the shape of agricultural materials using spherical harmonics." **Computers and Electronics in Agriculture**. 128 : 160-171.

[11] Aguilera, J.M and Stanley, D.W. **Microstructural Principles of Food Processing and Engineering.** 2nd ed. Gaithersburg : Aspen Publication. 1999.

[12] Russ, C.J. **The Image Processing Handbook**. 5th ed. Boca Raton : CRC Press. 2007.

[13] Ratti, C. Editors. **Advances in Food Dehydration**. Boca Raton : CRC Press. 2008.

[14] Neal, F.B. and Russ, C.J. **Measuring Shapes.** Boca Raton : CRC Press. 2012.

[15] Schanda, J. **Colorimetry: Understanding the CIE System**. Hoboken : John Wiley & Sons, Inc. 2007.

[16] ASTM E179. **Standard Guide for Selection of Geometric Conditions for Measurement of Reflection and Transmission Properties of Materials**. West Conshohocken : ASTM International. 2017.

[17] Hunter Associates Laboratory Inc. "**CIE Standard Observers and calculation of CIE X, Y, Z color values.**" [Online]. Available : https://www.hunterlab.com/duplicate-of-an-1002.01-standard-observer.pdf. 2015.

[18] Whetzel, N. "**Light Sources and Illuminants.**" [Online]. Available : https://support.hunterlab.com/hc/en-us/articles/202021855-Light-Sources-and-Illuminants. 2015.

[19] Fernández, L., Castillero, C. and Aguilera, J.M. 2005. "An application of image analysis to dehydration of apple discs." **Journal of Food Engineering**. 67(1-2) : 185-193.

[20] Igathinathane, C., Pordesimo, L.O., Columbus, E.P., Batchelor, W.D. and Sokhansanj, S. 2009. "Sieveless particle size distribution analysis of particulate materials through computer vision." **Computers and Electronics in Agriculture**. 66(2) : 147-158.

[21] Difference Between. "**Difference between CCD and CMOS Sensor.**" [Online]. Available : http://www.differencebetween.info/difference-between-ccd-vs-cmos-sensor. 2017.

[22] Mansurov, N. "**Understanding Aperture – A Beginner's Guide.**" [Online]. Available : https://photographylife.com/what-is-aperture-in-photography. 2017.

[23] Mansurov, N. “**Understanding Shutter Speed – A Beginner’s Guide**.” [Online]. Available : https://photographylife.com/what-is-shutter-speed-in-photography. 2017.

[24] Mansurov, N. “**Understanding ISO – A Beginner’s Guide**.” [Online]. Available : https://photographylife.com/what-is-iso-in-photography. 2017.

[25] Peters, D. “**Genialer Spickzettel für Fotografen.**” [Online]. Available : https://www.hamburger-fotospots.de/kostenloser-download-foto-cheatcard-fuer-fotografen.html. 2017.

[26] Otsu, N. 1979. “A Thershold Selection Method from Gray-Level Histrograms.” **IEEE Transactions on Systems**. 9(1) : 62-66.

[27] Greensted, A. “**Otsu Thresholding**.” [Online]. Available : http://www.labbookpages.co.uk/software/imgProc/otsuThreshold.html. 2010.

[28] MathWorks, Inc. “**Image Processing Toolbox™: User’s Guide (R2017b).**” [Online]. Available : https://www.mathworks.com/help/releases/R2017b/pdf_doc/images/images_tb.pdf. 2017.

[29] Igathinathane, C., Pordesimo, L.O., Columbus, E.P., Batchelor, W.D. and Methuku, S.R. 2008. “Shape identification and particles size distribution from basic shape parameters using ImageJ.” **Computers and Electronics in Agriculture**. 63(2) : 168-182.

[30] Ferreira, T. and Rasband, W. “**ImageJ User Guide (IJ 1.46r).**” [Online]. Available : https://imagej.nih.gov/ij/docs/guide/user-guide.pdf. 2012.

[31] Liu, E.J., Cashman, K.V. and Rust, A.C. 2015. “Optimising shape analysis to quantify volcanic ash morphology.” **GeoResJ**. 8 : 14-30.

[32] Montgomery, D.C., Runger, G.C. and Hubele, N.F.. **Engineering Statistics** 5th ed. Hoboken : John Wiley and Sons, Inc. 2010.

[33] Agisoft LLC. “**Agisoft PhotoScan User Manual: Standard Edition (Version 1.4).**” [Online]. Available : http://www.agisoft.com/pdf/photoscan_1_4_en.pdf. 2018.

APPENDIX

APPENDIX A

Changes of Agar of Different Sugar Contents during Drying at Different Temperatures

A.1 Moisture content of agar of different sugar contents during drying at different temperatures

Table A.1 Moisture content (d.b) ($g_{water}/g_{bone\ dry\ mass}$) of agar of different sugar contents during drying at 80 °C

	0%				10%				20%			
Time (min)	1	2	Avg.	SD	1	2	Avg.	SD	1	2	Avg.	SD
0	45.50	44.71	45.11	0.40	4.98	4.81	4.89	0.08	2.92	2.61	2.77	0.16
60	37.43	40.98	39.21	1.78	4.30	4.07	4.18	0.12	2.45	2.47	2.46	0.01
120	31.67	35.95	33.81	3.02	3.74	3.50	3.62	0.12	2.16	2.18	2.17	0.01
180	26.49	31.02	28.75	3.20	3.41	3.25	3.33	0.08	1.91	1.96	1.94	0.03
240	19.96	29.56	24.76	6.79	2.92	3.02	2.97	0.05	1.71	1.82	1.77	0.08
300	15.78	23.07	19.43	5.16	2.56	2.43	2.49	0.06	1.44	1.51	1.48	0.05
360	10.02	17.52	13.77	5.31	2.21	2.17	2.19	0.02	1.19	1.30	1.24	0.07
420	5.52	17.70	11.61	8.62	1.92	1.42	1.67	0.25	1.09	1.27	1.18	0.13
480	2.16	11.57	6.87	6.65	1.35	1.24	1.29	0.06	0.98	1.09	1.03	0.08
540	1.09	4.42	2.76	2.35	1.13	0.96	1.05	0.08	0.82	0.96	0.89	0.09

Table A.2 Moisture content (d.b) ($g_{water}/g_{bone\ dry\ mass}$) of agar of different sugar contents during drying at 60 °C

	0%				20%			
Time (min)	1	2	Avg.	SD	1	2	Avg.	SD
0	45.50	44.71	45.11	0.40	2.92	2.61	2.77	0.16
60	43.94	42.38	43.16	1.10	2.74	2.92	2.83	0.13
120	40.63	39.21	39.92	1.01	2.44	2.64	2.54	0.14
180	37.66	35.71	36.68	1.38	2.15	2.34	2.24	0.13
240	34.14	33.24	33.69	0.63	1.79	2.21	2.00	0.29
300	28.62	30.57	29.60	1.38	1.76	1.97	1.86	0.15
360	25.62	27.16	26.39	1.09	1.59	1.68	1.63	0.06
420	20.21	21.83	21.02	1.15	1.24	1.70	1.47	0.33
480	17.30	20.29	18.79	2.11	1.34	1.61	1.48	0.19
540	16.87	17.75	17.31	0.44	1.22	1.59	1.41	0.19

A.2 Volume (from liquid displacement method) of agar of different sugar contents during drying at different temperatures

Table A.3 Volume (liquid displacement) (mm^3) of agar of different sugar contents during drying at 80 °C

	0%				10%				20%			
Time (min)	1	2	Avg.	SD	1	2	Avg.	SD	1	2	Avg.	SD
0	7025.08	7227.01	7126.04	142.79	7121.77	7579.59	7350.68	228.91	7683.38	7896.69	7790.04	150.83
60	6669.64	6311.28	6490.47	179.18	6309.97	6643.13	6476.55	166.58	6842.51	6221.35	6531.95	310.58
120	4880.98	5365.10	5123.04	342.32	5752.14	5522.44	5637.29	114.85	6400.20	5103.98	5752.09	916.57
180	4051.82	4888.33	4470.08	591.50	4583.10	5124.84	4853.97	270.87	5225.68	4951.19	5088.43	194.09
240	3039.79	4659.98	3849.88	1145.65	4519.13	4580.05	4549.59	30.46	4465.06	4531.93	4498.50	47.28
300	2394.52	3627.55	3011.03	871.89	3809.67	3561.61	3685.64	124.03	3793.71	3638.25	3715.98	109.93
360	1495.15	2742.90	2119.02	882.29	3265.58	3079.55	3172.56	93.01	3017.05	3053.83	3035.44	26.01
420	743.23	2753.59	1748.41	1421.54	2757.12	1948.49	2352.81	404.32	2704.78	2941.49	2823.14	167.38
480	336.90	1786.02	1061.46	1024.69	2119.95	1620.03	1869.99	249.96	2336.50	2452.69	2394.60	82.16
540	81.25	845.72	463.49	540.56	1698.14	1220.46	1459.30	238.84	1885.65	2177.96	2031.81	206.69

Table A.4 Volume (liquid displacement) (mm^3) of agar of different sugar contents during drying at 60 ℃

	0%				20%			
Time (min)	1	2	Avg.	SD	1	2	Avg.	SD
0	6540.33	7293.55	6916.94	532.60	6813.67	6842.53	6828.10	20.41
60	6639.33	6529.25	6584.29	77.84	7051.33	7272.15	7161.74	156.14
120	7263.00	6381.48	6822.24	623.33	7063.67	6504.18	6783.92	395.62
180	5096.61	5818.46	5457.53	510.42	6210.85	5694.75	5952.80	364.94
240	5390.75	5406.89	5398.82	11.41	4792.40	5334.34	5063.37	383.21
300	4461.95	4991.64	4726.80	374.55	4353.28	4695.75	4524.51	242.17
360	3990.79	4406.89	4198.84	294.23	3879.31	3892.68	3885.99	9.45
420	3435.89	3517.22	3476.55	57.51	2911.05	3872.95	3392.00	680.17
480	2695.20	3250.42	2972.81	392.60	3145.07	3657.31	3401.19	362.21
540	6540.33	2781.68	6916.94	532.60	6813.67	3130.06	3130.06	20.41

A.3 Average values of parameters from 2D Image analysis of agar with 0% sugar during drying at 80 °C

Table A.5 2D image analysis parameters of agar with 0% sugar during drying at 80 °C

	Image parameter					
Time (min)	Projected area (pixel)	Perimeter (pixel)	Major Axis (pixel)	Minor Axis (pixel)	Max Feret Diameter (pixel)	Min Feret Diameter (pixel)
0	90524.67 ± 524.67	1194.45 ± 5.55	352.25 ± 2.25	345.24 ± 4.76	357.80 ± 7.80	297.14 ± 2.86
60	76805.17 ± 1805.17	1037.81 ± 37.81	321.50 ± 6.50	315.20 ± 0.20	327.04 ± 12.04	277.17 ± 2.17
120	65612.00 ± 4313.00	976.69 ± 25.24	296.32 ± 10.01	290.34 ± 9.74	304.92 ± 7.92	255.09 ± 9.61
180	59260.33 ± 3832.67	922.53 ± 32.53	281.61 ± 9.27	275.15 ± 9.23	289.18 ± 9.43	244.33 ± 6.16
240	52988.67 ± 6833.00	878.85 ± 52.95	264.21 ± 17.23	261.07 ± 17.64	274.26 ± 19.93	231.57 ± 14.5
300	47287.00 ± 5458.33	829.82 ± 41.65	251.69 ± 13.55	244.67 ± 15.05	257.36 ± 14.35	216.70 ± 15.34
360	39426.33 ± 6053.00	762.60 ± 51.01	231.72 ± 14.82	220.61 ± 19.36	239.49 ± 14.24	196.92 ± 14.37
420	37955.00 ± 6816.33	747.53 ± 60.47	228.03 ± 16.52	215.53 ± 22.94	234.99 ± 17.47	195.08 ± 18.64
480	34949.33 ± 4491.33	750.79 ± 49.03	222.65 ± 11.11	205.28 ± 16.56	221.42 ± 15.8	174.36 ± 11.00
540	30780.83 ± 4027.83	714.28 ± 77.56	207.35 ± 12.39	193.16 ± 14.53	215.73 ± 13.66	177.05 ± 11.85

Table A.6 2D image analysis parameters of agar with 0% sugar during drying at 80 °C (cont'd)

Time (min)	Image parameter					
	Bounding box length (pixel)	Bounding box width(pixel)	Bounding box area (pixel)	Convex area (pixel)	Bounding box perimeter (pixel)	Convex perimeter (pixel)
0	321.17 ± 1.17	310.50 ± 0.50	99716.50 ± 516.50	93944.50 ± 55.50	1263.33 ± 3.33	1181.56 ± 18.44
60	300.33 ± 0.33	290.00 ± 1.00	87113.17 ± 186.83	77630.67 ± 2630.67	1180.67 ± 1.33	1032.15 ± 32.15
120	267.83 ± 4.83	269.67 ± 1.00	72262.83 ± 1555.17	66649.33 ± 4004.33	1075.00 ± 11.67	968.79 ± 28.82
180	254.00 ± 6.67	254.67 ± 11.33	64845.83 ± 4577.50	60164.00 ± 3917.33	1017.33 ± 36.00	916.70 ± 32.75
240	243.00 ± 11.00	244.33 ± 9.67	59494.67 ± 5028	54282.00 ± 6473.33	974.67 ± 41.33	866.75 ± 58.48
300	231.33 ± 12.67	232.67 ± 12.33	54046.17 ± 5849.17	48662.17 ± 5056.50	928.00 ± 50.00	816.97 ± 46.59
360	220.67 ± 10.67	213.67 ± 15.33	47335.33 ± 5694.33	41064.00 ± 5852.33	868.67 ± 52.00	744.62 ± 56.10
420	215.17 ± 14.50	213.17 ± 23.17	46242.67 ± 8079.67	39521.33 ± 6581.00	856.67 ± 75.33	730.06 ± 66.06
480	209.33 ± 10.33	210.33 ± 14.33	44161.00 ± 5186.33	37780.67 ± 4703.33	839.33 ± 49.33	709.97 ± 50.93
540	215.50 ± 20.83	208.33 ± 17.33	45303.83 ± 7987.83	33528.50 ± 5160.17	847.67 ± 76.33	665.90 ± 51.51

Table A.7 2D image analysis parameters of agar with 0% sugar during drying at 80 °C (cont'd)

Time (min)	Image parameter						
	Max radius (pixel)	Min radius (pixel)	Mean radius (pixel)	SD radius (pixel)	Equivalent diameter (pixel)	Ellipse Area (pixel)	Area/ perimeter (pixel)
0	209.88 ± 0.12	148.14 ± 1.86	170.82 ± 0.82	35.92 ± 0.08	265.73 ± 74.75	94891.89 ± 108.11	75.79 ± 0.79
60	193.70 ± 1.30	138.67 ± 1.33	159.77 ± 0.23	30.59 ± 0.59	245.35 ± 71.01	80625.17 ± 625.17	74.04 ± 0.96
120	173.35 ± 5.61	126.45 ± 4.91	146.55 ± 5.49	27.18 ± 0.57	288.85 ± 9.48	67661.66 ± 4560.48	67.10 ± 2.67
180	164.19 ± 6.29	120.32 ± 3.56	138.81 ± 4.32	25.29 ± 1.38	274.39 ± 8.91	60992.08 ± 4035.34	64.10 ± 1.90
240	155.86 ± 13.66	114.15 ± 7.25	131.38 ± 8.99	23.85 ± 3.20	259.18 ± 16.78	54419.10 ± 7195.26	60.04 ± 4.16
300	147.12 ± 6.45	107.39 ± 7.03	123.54 ± 7.07	22.60 ± 0.18	244.84 ± 14.12	48573.73 ± 5607.34	56.75 ± 3.69
360	133.65 ± 9.07	95.62 ± 9.66	112.28 ± 8.97	22.19 ± 0.57	223.15 ± 17.05	40454.38 ± 6170.76	51.30 ± 4.41
420	131.82 ± 11.64	93.01 ± 11.90	110.04 ± 10.04	22.59 ± 0.98	218.89 ± 19.81	38911.92 ± 6912.65	50.35 ± 5.04
480	128.09 ± 10.14	84.36 ± 6.99	105.84 ± 7.18	26.49 ± 1.27	210.43 ± 13.52	36059.19 ± 4707.79	46.34 ± 2.94
540	118.31 ± 8.41	81.02 ± 5.21	99.15 ± 6.74	22.59 ± 1.96	197.45 ± 13.02	31620.68 ± 4232.76	43.08 ± 1.11

Table A.8 2D image analysis parameters of agar with 0% sugar during drying at 80 °C (cont'd)

Time (min)	Image parameter					
	Form factor	Roundness	Aspect ratio	$Extent_{box}$	$Extent_{max}$	Solidity
0	0.815 ± 0.005	0.869 ± 0.001	1.236 ± 0.006	0.904 ± 0.004	0.659 ± 0.001	0.965 ± 0.005
60	0.856 ± 0.002	0.880 ± 0.010	1.217 ± 0.003	0.903 ± 0.003	0.674 ± 0.004	0.970 ± 0.010
120	0.863 ± 0.012	0.897 ± 0.012	1.196 ± 0.014	0.909 ± 0.039	0.694 ± 0.001	0.984 ± 0.006
180	0.874 ± 0.005	0.901 ± 0.001	1.183 ± 0.009	0.915 ± 0.005	0.699 ± 0.008	0.985 ± 0.001
240	0.858 ± 0.008	0.894 ± 0.014	1.184 ± 0.012	0.888 ± 0.040	0.695 ± 0.032	0.975 ± 0.010
300	0.859 ± 0.012	0.906 ± 0.004	1.189 ± 0.018	0.876 ± 0.007	0.692 ± 0.020	0.971 ± 0.011
360	0.844 ± 0.016	0.868 ± 0.028	1.219 ± 0.015	0.828 ± 0.027	0.697 ± 0.012	0.958 ± 0.010
420	0.845 ± 0.016	0.867 ± 0.027	1.207 ± 0.026	0.823 ± 0.005	0.689 ± 0.003	0.958 ± 0.013
480	0.776 ± 0.002	0.908 ± 0.009	1.270 ± 0.010	0.790 ± 0.008	0.679 ± 0.019	0.924 ± 0.003
540	0.769 ± 0.061	0.843 ± 0.001	1.220 ± 0.002	0.689 ± 0.036	0.700 ± 0.007	0.922 ± 0.022

Table A.9 2D image analysis parameters of agar with 0% sugar during drying at 80 °C (cont'd)

	Image parameter					
Time (min)	$Convexity_{cvx}$	Eccentricity	Radius ratio	Shape factor	Perim/maxR	FD
0	1.026 ± 0.004	1.393 ± 0.007	0.699 ± 0.001	0.204 ± 0.004	1.812 ± 0.008	2.387 ± 0.313
60	1.015 ± 0.005	1.394 ± 0.006	0.712 ± 0.002	0.193 ± 0.003	1.795 ± 0.015	2.061 ± 0.001
120	1.008 ± 0.004	1.400 ± 0.001	0.729 ± 0.005	0.186 ± 0.003	1.794 ± 0.012	2.050 ± 0.002
180	1.006 ± 0.001	1.398 ± 0.001	0.733 ± 0.006	0.182 ± 0.004	1.789 ± 0.005	2.043 ± 0.005
240	1.014 ± 0.007	1.406 ± 0.002	0.734 ± 0.018	0.181 ± 0.012	1.799 ± 0.050	2.036 ± 0.007
300	1.016 ± 0.007	1.394 ± 0.005	0.730 ± 0.016	0.184 ± 0.012	1.795 ± 0.012	2.030 ± 0.007
360	1.025 ± 0.009	1.380 ± 0.015	0.713 ± 0.023	0.200 ± 0.021	1.818 ± 0.001	2.021 ± 0.007
420	1.025 ± 0.010	1.375 ± 0.022	0.703 ± 0.028	0.208 ± 0.028	1.806 ± 0.013	2.017 ± 0.010
480	1.058 ± 0.007	1.359 ± 0.019	0.659 ± 0.002	0.251 ± 0.005	1.871 ± 0.023	2.022 ± 0.006
540	1.070 ± 0.034	1.367 ± 0.010	0.688 ± 0.006	0.227 ± 0.005	1.916 ± 0.071	2.016 ± 0.015

Table A.10 2D image analysis parameters of agar with 0% sugar during drying at 80 °C (cont'd)

Time (min)	Image parameter					
	Entirety	Circularity	$Convexity_{max}$	Axial ratio	Elongation	$Rectangularity_{box}$
0	0.036 ± 0.004	1.121 ± 0.009	0.968 ± 0.002	0.963 ± 0.002	1.464 ± 0.004	0.939 ± 0.001
60	0.026 ± 0.004	1.091 ± 0.009	0.990 ± 0.001	0.966 ± 0.004	1.461 ± 0.001	0.906 ± 0.006
120	0.016 ± 0.006	1.076 ± 0.008	0.981 ± 0.001	0.980 ± 0.001	1.420 ± 0.019	0.909 ± 0.013
180	0.015 ± 0.001	1.070 ± 0.003	0.985 ± 0.003	0.977 ± 0.001	1.414 ± 0.001	0.907 ± 0.001
240	0.026 ± 0.010	1.080 ± 0.005	0.980 ± 0.012	0.988 ± 0.002	1.424 ± 0.023	0.901 ± 0.016
300	0.031 ± 0.012	1.079 ± 0.008	0.974 ± 0.005	0.972 ± 0.007	1.406 ± 0.006	0.895 ± 0.003
360	0.045 ± 0.011	1.089 ± 0.010	0.987 ± 0.007	0.951 ± 0.022	1.472 ± 0.049	0.877 ± 0.006
420	0.044 ± 0.014	1.088 ± 0.010	0.988 ± 0.006	0.943 ± 0.032	1.472 ± 0.048	0.874 ± 0.006
480	0.082 ± 0.004	1.136 ± 0.002	0.926 ± 0.005	0.920 ± 0.028	1.408 ± 0.019	0.894 ± 0.006
540	0.087 ± 0.027	1.149 ± 0.051	0.955 ± 0.041	0.931 ± 0.014	1.520 ± 0.007	0.842 ± 0.016

Table A.11 2D image analysis parameters of agar with 0% sugar during drying at 80 °C (cont'd)

Time (min)	Image parameter						
	$Extent_{max,min}$	Paris factor	Concavity	$Rectangularity_{ef}$	Feret major ratio	Major/Perim	Square-circularity
0	0.848 ± 0.002	0.042 ± 0.002	0.048 ± 0.002	0.948 ± 0.002	0.830 ± 0.001	0.299 ± 0.001	1.213 ± 0.023
60	0.840 ± 0.010	0.021 ± 0.001	0.032 ± 0.008	0.938 ± 0.002	0.851 ± 0.001	0.302 ± 0.002	1.176 ± 0.004
120	0.843 ± 0.001	0.016 ± 0.008	0.026 ± 0.004	0.937 ± 0.042	0.861 ± 0.003	0.303 ± 0.002	1.159 ± 0.016
180	0.837 ± 0.006	0.013 ± 0.001	0.022 ± 0.003	0.941 ± 0.004	0.868 ± 0.007	0.305 ± 0.001	1.145 ± 0.006
240	0.831 ± 0.005	0.029 ± 0.015	0.034 ± 0.014	0.911 ± 0.044	0.877 ± 0.002	0.301 ± 0.002	1.166 ± 0.011
300	0.846 ± 0.010	0.032 ± 0.013	0.041 ± 0.011	0.900 ± 0.007	0.860 ± 0.015	0.303 ± 0.001	1.165 ± 0.017
360	0.830 ± 0.016	0.051 ± 0.017	0.054 ± 0.013	0.850 ± 0.026	0.849 ± 0.007	0.304 ± 0.001	1.187 ± 0.022
420	0.821 ± 0.008	0.050 ± 0.020	0.047 ± 0.012	0.845 ± 0.004	0.854 ± 0.020	0.305 ± 0.003	1.184 ± 0.022
480	0.906 ± 0.002	0.116 ± 0.013	0.115 ± 0.003	0.815 ± 0.010	0.782 ± 0.010	0.297 ± 0.005	1.291 ± 0.004
540	0.807 ± 0.001	0.139 ± 0.067	0.109 ± 0.045	0.707 ± 0.034	0.853 ± 0.006	0.292 ± 0.014	1.326 ± 0.120

A.4 Average values of parameters from 3D Image analysis of agar with 0% sugar during drying at 80 °C

Table A.12 3D image analysis parameters of agar with 0% sugar during drying at 80 °C

	Image parameter				
Time (min)	V/V_0	SA/S_0	SA Sphere/SA $Sphere_0$	Min R (voxel)	Max R (voxel)
0	1	1	1	6.430 ± 0.070	13.492 ± 0.092
60	0.760 ± 0.013	0.788 ± 0.033	0.833 ± 0.008	6.432 ± 0.118	13.912 ± 0.088
120	0.705 ± 0.025	0.736 ± 0.020	0.792 ± 0.019	6.465 ± 0.163	10.917 ± 0.145
180	0.576 ± 0.136	0.639 ± 0.082	0.688 ± 0.109	5.957 ± 0.993	10.401 ± 0.579
240	0.487 ± 0.065	0.570 ± 0.061	0.617 ± 0.056	5.430 ± 0.038	9.855 ± 1.060
300	0.366 ± 0.044	0.470 ± 0.037	0.510 ± 0.041	5.338 ± 0.370	8.996 ± 0.092
360	0.249 ± 0.062	0.373 ± 0.061	0.393 ± 0.066	4.195 ± 0.280	8.242 ± 0.835
420	0.266 ± 0.151	0.379 ± 0.141	0.397 ± 0.16	4.288 ± 1.296	8.150 ± 1.369
480	0.152 ± 0.057	0.283 ± 0.062	0.280 ± 0.072	3.273 ± 0.710	7.249 ± 0.876

Table A.13 3D image analysis parameters of agar with 0% sugar during drying at 80 °C (cont'd)

Time (min)	Image parameter					
	D_1 (voxel)	D_2 (voxel)	D_3 (voxel)	$D_1/(D_1+D_2+D_3)$	$D_2/(D_1+D_2+D_3)$	$D_3/(D_1+D_2+D_3)$
0	20.108 ± 0.108	19.361 ± 0.361	19.920 ± 0.080	0.338 ± 0.001	0.406 ± 0.077	0.647 ± 0.314
60	19.098 ± 0.098	17.741 ± 0.259	22.925 ± 0.075	0.324 ± 0.002	0.377 ± 0.081	0.741 ± 0.363
120	17.682 ± 0.104	16.976 ± 0.075	17.281 ± 0.251	0.341 ± 0.001	0.327 ± 0.001	0.333 ± 0.002
180	16.379 ± 1.163	16.165 ± 1.075	16.857 ± 1.148	0.332 ± 0.001	0.327 ± 0.001	0.341 ± 0.001
240	15.498 ± 1.220	14.942 ± 0.609	15.354 ± 0.832	0.338 ± 0.007	0.326 ± 0.006	0.336 ± 0.001
300	13.927 ± 1.002	13.797 ± 0.983	14.152 ± 0.254	0.332 ± 0.010	0.329 ± 0.010	0.339 ± 0.020
360	12.402 ± 1.878	12.185 ± 1.190	12.725 ± 0.798	0.330 ± 0.016	0.327 ± 0.002	0.343 ± 0.014
420	12.796 ± 2.814	13.026 ± 2.498	11.417 ± 2.114	0.342 ± 0.007	0.349 ± 0.004	0.309 ± 0.003
480	11.714 ± 1.171	11.726 ± 1.884	10.351 ± 0.655	0.347 ± 0.004	0.345 ± 0.018	0.308 ± 0.014

Table A.14 3D image analysis parameters of agar with 0% sugar during drying at 80 °C (cont'd)

Time (min)	Image parameter					
	Sphericity	Wadell's Sphericity	Scaling Factor	Radius ratio	Hoffmann shape entropy	Wadell's roundness
0	0.929 ± 0.021	0.864 ± 0.003	5.599 ± 0.015	0.477 ± 0.008	0.999 ± 0.001	0.787 ± 0.013
60	0.956 ± 0.005	0.913 ± 0.009	5.296 ± 0.021	0.462 ± 0.006	0.993 ± 0.007	0.718 ± 0.018
120	0.964 ± 0.002	0.929 ± 0.003	5.206 ± 0.017	0.592 ± 0.023	1.000 ± 0.001	0.735 ± 0.086
180	0.962 ± 0.015	0.926 ± 0.028	5.227 ± 0.159	0.569 ± 0.064	1.000 ± 0.001	0.740 ± 0.082
240	0.968 ± 0.009	0.938 ± 0.017	5.160 ± 0.091	0.558 ± 0.064	0.999 ± 0.001	0.706 ± 0.064
300	0.968 ± 0.001	0.937 ± 0.003	5.160 ± 0.014	0.593 ± 0.035	0.998 ± 0.001	0.742 ± 0.090
360	0.954 ± 0.002	0.910 ± 0.004	5.313 ± 0.023	0.511 ± 0.018	0.999 ± 0.001	0.704 ± 0.066
420	0.944 ± 0.018	0.892 ± 0.034	5.427 ± 0.207	0.514 ± 0.073	0.997 ± 0.002	0.751 ± 0.053
480	0.920 ± 0.019	0.847 ± 0.036	5.723 ± 0.240	0.446 ± 0.044	0.998 ± 0.001	0.712 ± 0.040

A.5 Image-based parameters of agar of different sugar contents during drying at different temperatures

Table A.15 $Extent_{box}$ of agar of different sugar contents during drying at different temperatures

Time (min)	80 °C												60 °C			
	0%				10%				20%				0%			
	1	2	Avg.	SD	1	2	Avg.	SD	1	2	Avg.	SD	1	2	Avg.	SD
0	0.90	0.92	0.91	0.01	0.91	0.93	0.92	0.01	0.88	0.86	0.87	0.01	0.68	0.85	0.77	0.08
60	0.92	0.91	0.91	0.01	0.86	0.85	0.86	0.01	0.88	0.87	0.87	0.01	0.73	0.87	0.80	0.07
120	0.87	0.95	0.91	0.04	0.88	0.81	0.85	0.04	0.80	0.88	0.84	0.04	0.85	0.79	0.82	0.03
180	0.92	0.91	0.91	0.01	0.82	0.90	0.86	0.04	0.83	0.84	0.84	0.01	0.76	0.82	0.79	0.03
240	0.85	0.93	0.89	0.04	0.91	0.92	0.91	0.01	0.83	0.93	0.88	0.05	0.93	0.88	0.90	0.03
300	0.87	0.88	0.88	0.01	0.92	0.91	0.92	0.01	0.85	0.87	0.86	0.01	0.78	0.90	0.84	0.06
360	0.80	0.85	0.83	0.03	0.88	0.84	0.86	0.02	0.87	0.89	0.88	0.01	0.75	0.84	0.79	0.04
420	0.82	0.83	0.82	0.01	0.85	0.80	0.82	0.02	0.83	0.87	0.85	0.02	0.88	0.90	0.89	0.01
480	0.78	0.80	0.79	0.01	0.88	0.82	0.85	0.03	0.83	0.89	0.86	0.03	0.75	0.89	0.82	0.07
540	0.72	0.65	0.69	0.04	0.87	0.76	0.81	0.06	0.83	0.85	0.84	0.01	0.88	0.90	0.89	0.01

Table A.16 Sphericity of agar of different sugar contents during drying at different temperatures

Time (min)	80 °C												60 °C			
	0%				10%				20%				0%			
	1	2	Avg.	SD	1	2	Avg.	SD	1	2	Avg.	SD	1	2	Avg.	SD
0	0.91	0.95	0.93	0.02	0.91	0.97	0.94	0.03	0.96	0.92	0.94	0.02	0.94	0.94	0.94	0.01
60	0.94	0.95	0.96	0.01	0.94	0.96	0.95	0.01	0.93	0.98	0.96	0.03	0.96	0.94	0.95	0.02
120	0.97	0.95	0.96	0.01	0.96	0.97	0.96	0.01	0.95	0.96	0.96	0.01	0.95	0.93	0.94	0.01
180	0.95	0.98	0.96	0.01	0.97	0.96	0.97	0.01	0.96	0.93	0.95	0.02	0.94	0.95	0.94	0.01
240	0.98	0.96	0.97	0.01	0.97	0.98	0.97	0.01	0.97	0.96	0.96	0.01	0.91	0.96	0.94	0.03
300	0.97	0.97	0.97	0.01	0.98	0.97	0.97	0.01	0.95	0.94	0.95	0.01	0.97	0.96	0.97	0.01
360	0.95	0.96	0.95	0.01	0.96	0.95	0.96	0.01	0.96	0.95	0.96	0.01	0.94	0.92	0.93	0.01
420	0.93	0.96	0.94	0.02	0.96	0.91	0.94	0.03	0.94	0.95	0.95	0.01	0.94	0.96	0.95	0.02
480	0.90	0.94	0.92	0.02	0.95	0.91	0.93	0.02	0.95	0.96	0.96	0.01	0.93	0.98	0.96	0.04

APPENDIX B
Developed Algorithms

B.1 2D Image Analysis

Adjust canvas size

%Change size of canvas of image to 512 pixel x 512 pixel

```
clear all
clc
% Running Program as batch
for i=1:11
        for j=1:3
                num1 = num2str(i-1);
                num2 = num2str(j);
                name = strcat(num1,' (',num2,')','.JPG');
                %If name of image exist, start the operation
                if exist(name,'file')>0
                        I = imread(name);
                        [x,y,~] = size(I);
                        xmustbe = 256-round(x/2);
                        ymustbe = 256-round(y/2);
                        I2 = padarray(I,[xmustbe,ymustbe],0,'both');
                        I2 = imcrop(I2,[1,1,512,512]);
                        imwrite(I2,name);
                end
        end
end
```

Diameter analysis

%This code is for finding radius and Feret diameter of binary image

```
function [ output_args ] = Diameter(I,command)
        a = regionprops(I,'BoundingBox');
        xs = a.BoundingBox(1);
        ys = a.BoundingBox(2);
```

```
xl = a.BoundingBox(3);
yl = a.BoundingBox(4);
Crop = imcrop(I,[xs ys xl yl]);
E = edge(Crop,'Canny');
[x y] = find(E == 1);
l = length(x);
xmid = round((max(x)+min(x))/2);
ymid = round((max(y)+min(y))/2);
for i = 1:l
        thetha(i,:) = (atan((y(i)-ymid)/(x(i)-xmid)));
        rho(i,:) = sqrt((x(i)-xmid).^2+(y(i)-ymid).^2);
end
for i = 1:l
        if thetha(i)>=0
                cothetha = thetha(i)-pi;
        else
                cothetha = thetha(i)+pi;
        end
        temp = abs(thetha-cothetha);
        [row col] = find(temp == min(temp));
        if length(row) == 1
                Diameter(i) = rho(i)+rho(row);
        else
                Diameter(i) = rho(i)+max(rho(row));
        end
end
switch command
        case 'MaxFeret'
                output_args = max(Diameter);
        case 'MinFeret'
                output_args = min(Diameter);
        case 'MeanFeret'
                output_args = mean(Diameter);
        case 'MaxR'
                output_args = max(rho);
        case 'MinR'
                output_args = min(rho);
        case 'MeanR'
```

```
                output_args = mean(rho);
        end
end
```

Fractal dimension analysis

```
%Find fractral dimension using box-counting method

function [n,r] = boxcount(c,varargin)
% control input argument
        error(nargchk(1,2,nargin));
        % check for true color image (m-by-n-by-3 array)
        if ndims(c)==3
                if size(c,3)==3 && size(c,1)>=8 && size(c,2)>=8
                        c = sum(c,3);
                end
        end
        warning off
        c = logical(squeeze(c));
        warning on
        dim = ndims(c); % dim is 2 for a vector or a matrix, 3 for a cube
        if dim>3
                error('Maximum dimension is 3.');
        end
        % transpose the vector to a 1-by-n vector
        if length(c)==numel(c)
                dim=1;
                if size(c,1)~=1
                        c = c';
                end
        end
        width = max(size(c));    % largest size of the box
        p = log(width)/log(2);   % nbre of generations
        % remap the array if the sizes are not all equal, or if they are not power of
        %two this slows down the computation!)
        if p~=round(p) || any(size(c)~=width)
                p = ceil(p);
                width = 2^p;
                switch dim
```

```
                case 1
                        mz = zeros(1,width);
                        mz(1:length(c)) = c;
                        c = mz;
                case 2
                        mz = zeros(width, width);
                        mz(1:size(c,1), 1:size(c,2)) = c;
                        c = mz;
                case 3
                        mz = zeros(width, width, width);
                        mz(1:size(c,1), 1:size(c,2), 1:size(c,3)) = c;
                        c = mz;
        end
end
n=zeros(1,p+1); % pre-allocate the number of box of size r
switch dim
        case 1      %------------------ 1D boxcount ---------------------%
        n(p+1) = sum(c);
        for g=(p-1):-1:0
                siz = 2^(p-g);
                siz2 = round(siz/2);
                for i=1:siz:(width-siz+1)
                        c(i) = ( c(i) || c(i+siz2));
                end
                n(g+1) = sum(c(1:siz:(width-siz+1)));
        end
        case 2      %------------------ 2D boxcount ---------------------%
        n(p+1) = sum(c(:));
                for g=(p-1):-1:0
                        siz = 2^(p-g);
                        siz2 = round(siz/2);
                        for i=1:siz:(width-siz+1)
                                for j=1:siz:(width-siz+1)
                                        c(i,j) = ( c(i,j) || c(i+siz2,j) ||...
                                         c(i,j+siz2) || c(i+siz2,j+siz2) );
                                end
                        end
                n(g+1) = sum(sum(c(1:siz:(width-siz+1),1:siz:(width-siz+1))));
```

```
                end
        case 3          %------------------ 3D boxcount ---------------------%
                n(p+1) = sum(c(:));
                for g=(p-1):-1:0
                        siz = 2^(p-g);
                        siz2 = round(siz/2);
                        for i=1:siz:(width-siz+1),
                                for j=1:siz:(width-siz+1),
                                        for k=1:siz:(width-siz+1),
                                                c(i,j,k)=( c(i,j,k) || c(i+siz2,j,k) ||...
                                                        c(i,j+siz2,k) ||...
                                                        c(i+siz2,j+siz2,k) |...|
                                                        c(i,j,k+siz2) ||...
                                                        c(i+siz2,j,k+siz2) ||...
                                                        c(i,j+siz2,k+siz2) ||...
                                                        c(i+siz2,j+siz2,k+siz2));
                                        end
                                end
                        end
                        n(g+1) = sum(sum(sum(c(1:siz:(width-siz+1),1:siz:(width-
                        siz+1),1:siz:(width-siz+1)))));
                end
        end
n = n(end:-1:1);
r = 2.^(0:p); % box size (1, 2, 4, 8...)
if any(strncmpi(varargin,'slope',1))
        s=-gradient(log(n))./gradient(log(r));
        semilogx(r, s, 's-');
        ylim([0 dim]);
        xlabel('r, box size'); ylabel('- d ln n / d ln r, local dimension');
        title([num2str(dim) 'D box-count']);
elseif nargout==0 || any(strncmpi(varargin,'plot',1))
        loglog(r,n,'s-');
        xlabel('r, box size'); ylabel('n(r), number of boxes');
        title([num2str(dim) 'D box-count']);
end
if nargout==0
        clear r n
```

```
        end
end
```

Reference : Moisy, F. 2008 **boxcount.** [Online].
Available :
https://www.mathworks.com/matlabcentral/fileexchange/13063-boxcount?focused=5083247&tab=example.

Parameter analysis

```
% For analyzing 2D image

clear all
clc
for n = 1:10
        for m = 1:3
                num1 = num2str(n-1);
                num2 = num2str(m);
                name = strcat(num1,'(',num2,')_BW.jpg');
                if exist(name) ~= 0
                        I = imread(name);
                        level = graythresh(I);
                        BW = im2bw(I,level);
                        BW1 = bwareaopen(BW,500);
                        E = edge(BW1,'Canny');
                        a1 = regionprops(BW1,'Area');
                        a2 = regionprops(BW1,'MajorAxisLength');
                        a3 = regionprops(BW1,'MinorAxisLength');
                        a4 = regionprops(BW1,'Perimeter');
                        a5 = regionprops(BW1,'BoundingBox');
                        a6 = regionprops(BW1,'ConvexImage');
                        CVXI = a6.ConvexImage;
                        a7 = regionprops(CVXI,'Area');
                        a8 = regionprops(CVXI,'Perimeter');
                        Area = a1.Area;
                        Perim = a4.Perimeter;
                        Major = a2.MajorAxisLength;
                        Minor = a3.MinorAxisLength;
                        MaxFeret = Diameter(BW1,'MaxFeret');
```

```
MinFeret = Diameter(BW1,'MinFeret');
BBL = a5.BoundingBox(3);
BBW = a5.BoundingBox(4);
AreaBox = BBL*BBW;
AreaCVX = a7.Area;
PerimBox = 2*(BBL+BBW);
PerimCVX = a8.Perimeter;
MaxR = Diameter(BW1,'MaxR');
MinR = Diameter(BW1,'MinR');
MeanR = Diameter(BW1,'MeanR');
DevR = sqrt((((MaxR-MinR)^2)-((MaxR-MeanR)^2))/2);
EquivDiameter = sqrt(4*Area/pi);
AreaEllispe = (pi/4)*(Major*Minor);
AreaperPerim = Area/Perim;
Answer1temp(m,:) = [Area Perim Major Minor MaxFeret
                    MinFeret BBL BBW AreaBox AreaCVX
                    PerimBox PerimCVX MaxR MinR MeanR.
                    DevR EquivDiameter AreaEllispe
                    AreaperPerim];
if m == 3
        Answer1(n,:) = mean(Answer1temp);
end
[count box] = boxcount(E);
Formfactor = (4*pi*Area)/(Perim^2);
Roundness = (4*Area)/(pi*(MaxFeret^2));
AspectRatio = MaxFeret/MinFeret;
Extent1 = Area/AreaBox;
Extent2 = Area/(pi*(MaxR^2));
Solidity = Area/AreaCVX;
Convexity1 = Perim/PerimCVX;
Eccentricity = (sqrt(Major^2+Minor^2))/Major;
RadiusRatio = MinR/MaxR;
SF = DevR/MeanR;
Ratio = Perim/MaxR;
FD = 1+mean(-gradient(log(count))./gradient(log(box)));
Entirety = (AreaCVX-Area)/Area;
Circularity = Perim/(2*sqrt(pi*Area));
Convexity2 = (pi*MaxFeret)/Perim;
```

```
                AxialRatio = Minor/Major;
                Elongation = (MaxFeret^2)/Area;
                Rectangularity1 = Perim/(PerimBox);
                Extent3 = Area/(MaxFeret*MinFeret);
                Paris = 2*((Perim-PerimCVX)/PerimCVX);
                Concavity = sqrt((1-Solidity)^2+(1-(1/Convexity2))^2);
                Rectangularity2 = AreaEllispe/(AreaBox);
                FeretMajor = MinFeret/Major;
                Annon1 = Major/Perim;
                Circularity2 = (Perim^2)/Area;
                Annon2 = (Perim-sqrt((Perim^2)-
                (4*pi*Area)))/(Perim+sqrt((Perim^2)-(4*pi*Area)));
                Temperature = 1/(log2((2*Perim)/(Perim-PerimCVX)));
                Answer2temp(m,:) = [Formfactor Roundness AspectRatio
                                    Extent1 Extent2 Solidity Convexity1
                                    Eccentricity RadiusRatio SF Ratio/pi FD
                                    Entirety Circularity Convexity2 AxialRatio
                                    Elongation Rectangularity1 Extent3 Paris
                                    Concavity Rectangularity2 FeretMajor
                                    Annon1 Circularity2/(4*pi) Annon2
                                    Temperature];
                if m == 3
                        Answer2(n,:) = mean(Answer2temp);
                end
            end
        end
end
```

B.2 3D Image Analysis

Image parameters analysis

%This code is for analyzing 3D image (point cloud file (.ply)). Unfortunately, volume, %surface area, sphericity, surface area of ellipse and Wadell's sphericity must be done %by COMSOL or %other program that can calculate mesh file

```
clear all
clc
m = 1;
for i = 0:8
        for a = 1:3
                num1 = num2str(i);
                num2 = num2str(a);
                name1 = strcat('H2-',num1,'-',num2,'.ply');
                name3 = strcat('H2-',num1,'-',num2,'.jpg');
                if exist(name1)~=0
                    I1 = pcread(name1);
                    Locate = double(I1.Location);
                    X_avg = mean(Locate(:,1));
                    Y_avg = mean(Locate(:,2));
                    Z_avg = mean(Locate(:,3));
                    X_new = Locate(:,1)-X_avg;
                    Y_new = Locate(:,2)-Y_avg;
                    Z_new = Locate(:,3)-Z_avg;
                    fig = scatter3(X_new,Y_new,Z_new);
                    saveas(fig,name2);
                    close(gcf);
                    [azimuth,elevation,r] = cart2sph(X_new,Y_new,Z_new);
                    r = r(r~=0);
                    azimuth = rad2deg(azimuth);
                    for j = 1:length(azimuth)
                            if azimuth(j) < 0
                                    azimuth(j) = abs(azimuth(j))+180;
                            end
                    end
                    elevation = rad2deg(elevation);
                    MinR = min(r);
```

```
                MaxR = max(r);
                MeanR = mean(r);
                SDR = std(r);
                RadiusRatio = MinR/MaxR;
                D1 = (I1.XLimits(2)-I1.XLimits(1));
                D2 = (I1.YLimits(2)-I1.YLimits(1));
                D3 = (I1.ZLimits(2)-I1.ZLimits(1));
                R1 = D1/(D1+D2+D3);
                R2 = D2/(D1+D2+D3);
                R3 = D3/(D1+D2+D3);
                Hoffmann =...
                (1/log(1/3))*((R1*(log(R1)))+(R2*(log(R2)))+(R3*(log(R3))));
                WadellRoundness = sum(sum(abs(r)))/(length(r)*max(r));
                Answer1(counter,:) = [MinR,MaxR,MeanR,SDR,R1,R2,R3];
                Answer2(counter,:) = [RadiusRatio,Hoffmann,WadellRoundness];
            else
                Answer1(counter,:) = zeros(1,7);
                Answer2(counter,:) = zeros(1,3);
            end
            counter = counter+1;
        end
end
```

AUTHOR BIOGRAPHY

Name	Miss Anyanun Stienkijumpai
Date of Birth	17 December 1991, Bangkok
Address	68/5, Soi Ekamai 4, Ekamai Rd., Phra Khanong Nuea, Wattana, Bangkok, 10110 Tel. 081 252 3236
Education Record	2014 Bachelor of Engineering (Food Engineering) (First Class Honors) King Mongkut's Institute of Technology Ladkrabang
Scholarship	Full tuition fee waiver scholarship from Faculty of Engineering, King Mongkut's Institute of Technology Ladkrabang
Publications	
International Journal	Jinorose, M., Stienkijumpai, A. and Devehastin, S. 2017. "Use of Image Analysis as a Monitoring Tool for Non-Uniform Deformation of Shrinkable Materials during Drying." **Journal of Chemical Engineering of Japan**. 50(10) : 785-791.
Conference	Stienkijumpai, A., Jinorose, M. and Devahastin, S. 2016. "Quantification of Non-Uniform Deformation of Shrinkable Materials during Drying via Digital image Analysis." in **Proceedings of the 20th International Drying Symposium**. August 7-10. Gifu, Japan.
Award Received	Best Research Award - In Recognition of Excellence in Drying Research, from the 20th International Drying Symposium (IDS 2016), August 7-10, 2016, Gifu, Japan.